SINTEF

SINTEF A17775 - Unrestricted

Report

Model Evaluation of Vesterålen and the Halten Bank

Final Report

Author(s)
Tron Vedul Tronstad
Jens M. Hovem

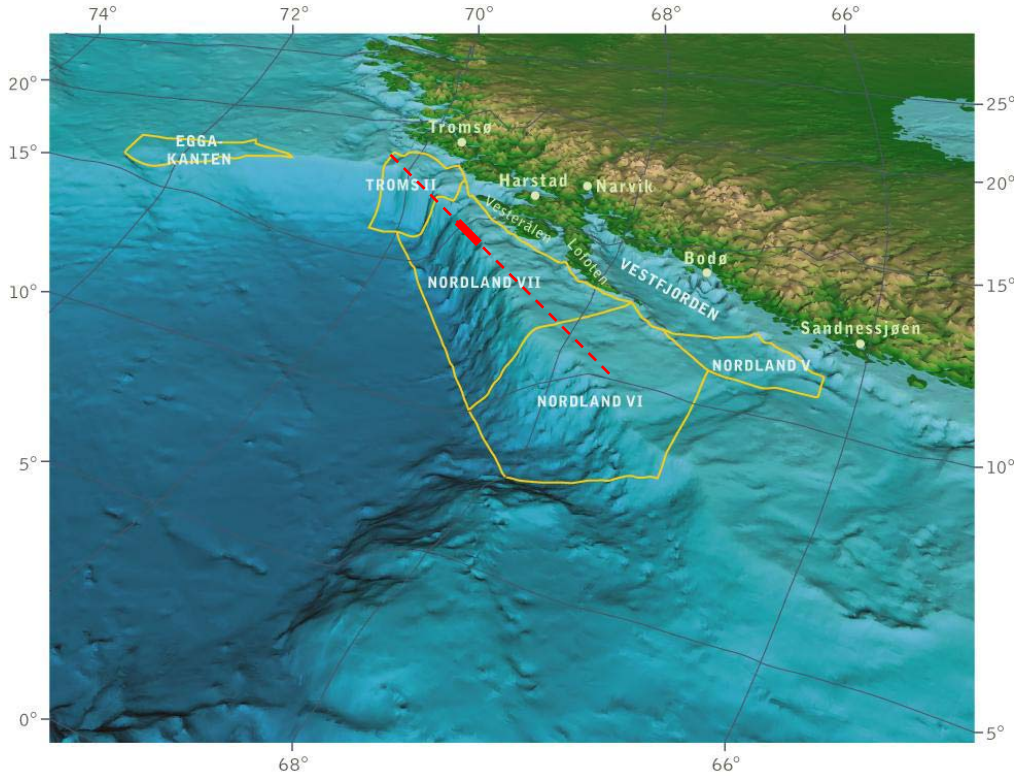

Picture from the Norwegian Petroleum Directorate (NPD) webpage. The solid red line illustrates the shooting line used in the modeling of Vesterålen. The dotted line illustrates the heading of this line.

SINTEF ICT
Acoustics
2011-01-20

SINTEF

SINTEF ICT
Address:
Postboks 4760 Sluppen
7465 Trondheim
NORWAY

Telephone:+47 73593000
Telefax:+47 73592730

postmottak.IKT@sintef.no
www.sintef.no
Enterprise /VAT No:
NO 948 007 029 MVA

Report

Model Evaluation of Vesterålen and the Halten Bank

Final Report

KEYWORDS:
Underwater sound propagation
Fish startle threshold
PlaneRay

VERSION
1.0

DATE
2011-01-20

AUTHOR(S)
Tron Vedul Tronstad
Jens M. Hovem

CLIENT(S)
The Norwegian Petroleum Directorate (NPD)

CLIENTS REF.
Jan Stenløkk

PROJECT NO.
90E322

NUMBER OF PAGES/APPENDICIES:
44+ Supplements

ABSTRACT

Model evaluation

This report describes the work and results of a computer program used to predict the propagation of air gun noise to long distances in the water column. The acoustic propagation model used is the PlaneRay model.
The sound levels found in the computer model was then used together with startle thresholds for cod. From this data we could find the distance where the sound level went below this threshold.
Probably, this is the first time a state-of- the-art propagation model is combined with current and advanced knowledge of fish hearing sensitivity to actually produce estimates of the minimum distance between seismic shooting and fish populations to avoid irregular behavior.

PROJECT MANAGER
Jens M. Hovem

SIGNATURE

CHECKED BY
Idar L. N. Granøien

SIGNATURE

APPROVED BY (name, position)
Odd Kr. Ø. Pettersen, Research Director

SIGNATURE

REPORT NO.
SINTEF A17775

ISBN
9788214049718

CLASSIFICATION
Unrestricted

CLASSIFICATION THIS PAGE
Unrestricted

Document history

VERSION	DATE	VERSION DESCRIPTION
0.1	2010-12-21	Initial draft
0.2	2011-01-13	Revised draft
1.0	2011-01-20	Final Report

SINTEF

Table of contents

Supplements

SINTEF

Model Evaluation of Vesterålen and the Halten Bank

1 Background and Introduction

The Norwegian Petroleum Directorate (NPD) commissioned SINTEF ICT and Department of Biology at the University of Oslo to develop an acoustic - biological model to predict the impact of seismic noise on the fish population. This report describes the work and results of SINTEF ICT in the development of a computer program to predict the propagation of air gun noise to long distances in the water column. The acoustic propagation model used is the PlaneRay model developed earlier, but adapted during the project to deal specifically with propagation of impulsive acoustic signals from air guns and air guns array

This model is based on ray theory and can deal with range-dependent bathymetry and depth-dependent sound speed profiles. The bottom is modeled as a sedimentary fluid layer over a solid elastic rock and the model requires the thickness and seismo-acoustic properties of the sediments layer and the rock with compressional speed, shear speed and absorption. The model simulates the total sound field, both in the time and in the frequency domain, out to very large distances. The model enables users to study the impact of airgun noise as function of seasonal environmental conditions at different geographical regions and sites.

The basic properties of the model are described in the SINTEF report A14560 “Mathematical modeling of seismic noise – model description and documentation”. Additional features regarding accuracy and modeling of air gun groups that were developed specifically is included as supplements or appendices in this report

The main objective of this report is to present results obtain by applying the model to realistic scenarios. First case treated is the analysis and modeling of a seismic line resulting from joint seismic-acoustic survey conducted in June 2009 at Vesterålen – Lofoten area (Nordland VII, see front page). In this experiment acoustic signals were recorded at a fixed position as the seismic vessel approached from a maximum distance of 30 km toward the receiving positions. The same situation was modeled using available geological and oceanographic information as input to the PlaneRay model. The agreement between the real and recorded signals and the model results is quite good, which indicates that the model can produce relevant results with sufficient accuracy.

Furthermore, this report contains a study of the importance of the seasonal variations that may occur in areas where seismic surveys may be conducted. Sound speed profile from the Halten bank at four different seasons were used to model time responses of the sound signals received near the bottom and higher up in the water column. The calculated sound exposure levels were compared with values of startle response levels for cod, provided by Department of Biology at the University of Oslo. A very preliminary conclusion indicates that the minimum required distance is in the range of 5 to 10 km, but dependent on the depth of the fish population and the season. In additions there will, under certain conditions, appear “hot spots” with significantly higher sound level due to caustics and focusing of sound.

Probably, this is the first time a state-of- the-art propagation model is combined with current and advanced knowledge of fish hearing sensitivity to actually produce estimates of the minimum distance between seismic shooting and fish populations to avoid irregular behavior.

1.1 Definitions

To describe the character of noise it is usual to use measures that describe the energy and peak content. In this study these descriptors have been sound exposure level (energy measure) and peak pressure level (peak content). These two descriptors are defined below.

1.1.1 Sound Exposure Level (SEL)

The *sound exposure level* is an energy based measure of noise often used to compare noise events of different length. The SEL value is equal to the level of a continuous noise of one second would have. It is defined as

$$\mathrm{SEL} = 10 \cdot \log_{10}\left[\frac{E_\mathrm{x}}{E_\mathrm{Ref}}\right] = 10 \cdot \log_{10}\left[\frac{E_\mathrm{x}}{p_\mathrm{Ref}^2 \cdot t_\mathrm{Ref}}\right]. \quad (1)$$

The sound exposure, E_x, is defined as

$$E_\mathrm{x} = \int_0^\mathrm{T} p^2(t)dt, \quad (2)$$

p_Ref is equal to 1 µPa and t_Ref is 1 second. SEL has the unit dB re ((1 µPa^2)(1 s)).

1.1.2 Peak Pressure Level (PPL)

Peak pressure level is another descriptor used to compare the maximum peak level of noise exposures. The PPL is defined as

$$\mathrm{PPL} = 20 \cdot \log_{10}\left[\frac{|p_\mathrm{max}|}{p_\mathrm{Ref}}\right], \quad (3)$$

where $|p_{max}|$ is the maximum peak value (absolute), and p_{ref} is equal to 1 µPa. PPL has the unit dB re 1 µPa.

2 The Seismic Survey in Vesterålen

During the summer in 2009 a seismic survey was performed outside Vesterålen in Norway. The survey was financed by the Norwegian Petroleum Directorate and was done by the vessel “Geo Pacific” using an array of air guns.

In connection with this survey the Institute of Marine Research had a project where they studied the effect this seismic shooting had on different commercial fish. To do this they also made recordings of the seismic shooting. In the next two sections these recordings have been used to compare real measurements with simulated results using PlaneRay [1], a ray tracing computer program for sound propagation.

The seismic survey was done in the fields Troms II and Nordland VII (see figure on front page), but the Institute of Marine Research did only collect data from Nordland VII to their study, hence the available recordings are from this region. The survey consists of several shooting lines and the recordings made were done at different location with both bottom hydrophones and using buoys floating on the surface.

2.1 Shooting Line 1344

We chose to model shooting line 1344 since the bottom hydrophone was placed almost directly below this line. This made it easier to extract depth information for the PlaneRay modeling. Other lines, e.g. surface hydrophones, would require the calculation of new depth profiles for each shot, a time consuming task.

The shooting line 1344 was also chosen because this line consisted of recordings with distances up to approximately 30 km.

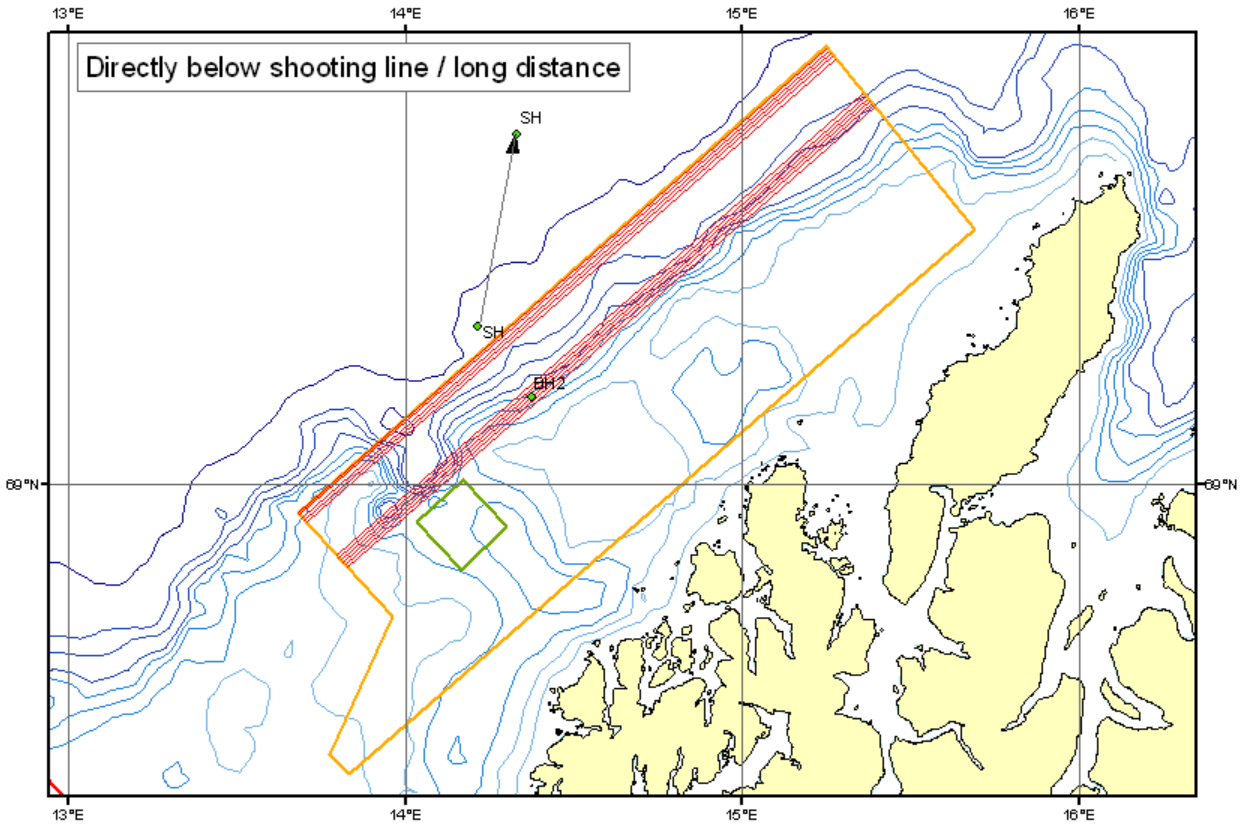

Figure 1 **Picture showing the location of the seismic survey – a selection of the field Nordland VII. The area inside the yellow line is the predetermined region of the study. The red lines are some of the shooting lines. BH2 is the location of one of the bottom hydrophone. SH is the drop point and the pickup point of a surface hydrophone. The arrow shows the drift of the buoy during the period of measurement.**

The location of the bottom hydrophone (BH2) can be seen in Figure 1. Shooting line 1344 is one of the red lines going directly over this hydrophone. As can be seen from the figure the shooting line is just on the edge of the continental shelf.

2.2 Bathymetry

To be able to model shooting line 1344 we needed the bathymetry of this line. Since the research vessel Geo Pacific recorded, among other details, the depth along the shooting line, we could extract this data directly from the log file. In addition we received depth information of the entire test region from the Norwegian Hydrographic Service. This data was used to create the illustration in Figure 2. This illustration also shows the drastic increase in depth outside the continental shelf, where the depth goes from around 300 – 500 m to above 2 500 m.

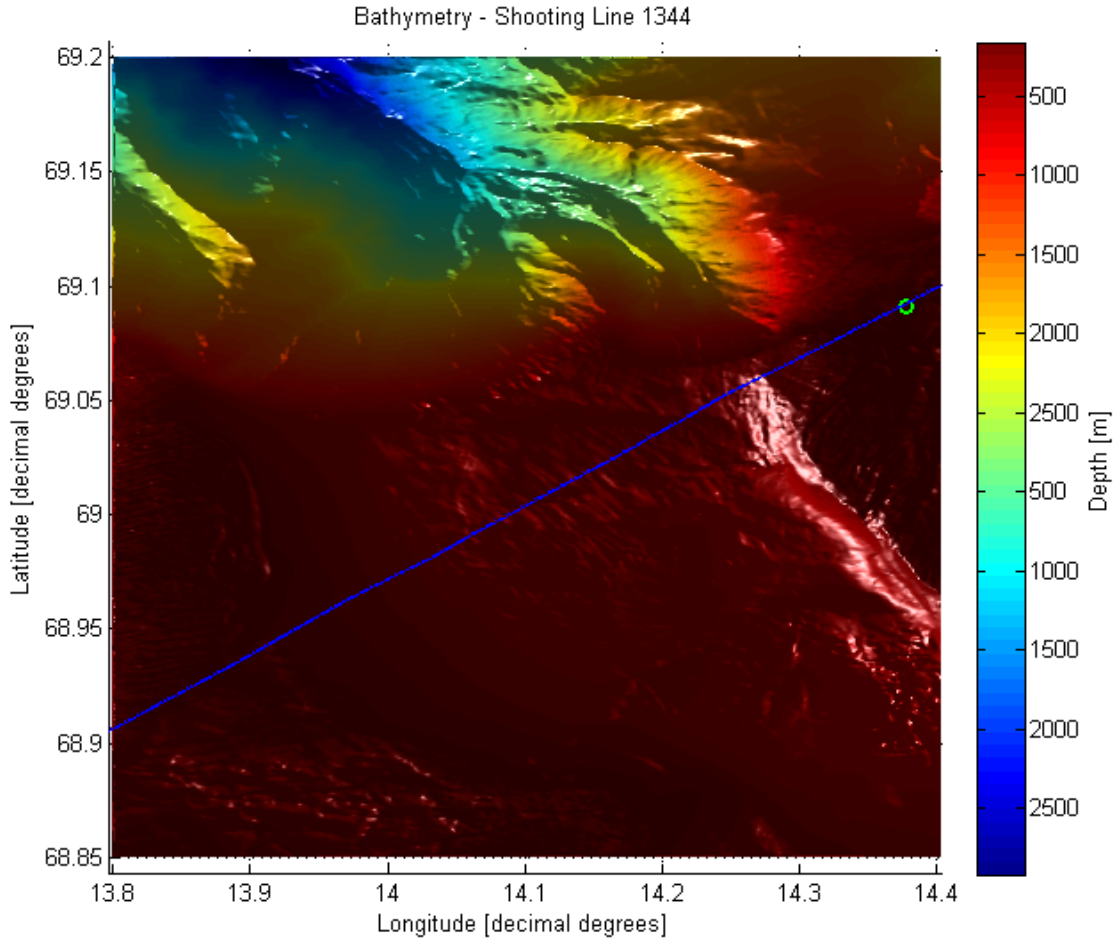

Figure 2 **Bathymetry of the seabed around shooting line 1344. The figure is also showing the shooting line (blue line) and the location of the bottom receiver 2 (green circle). Depth data from the Norwegian Hydrographic Service.**

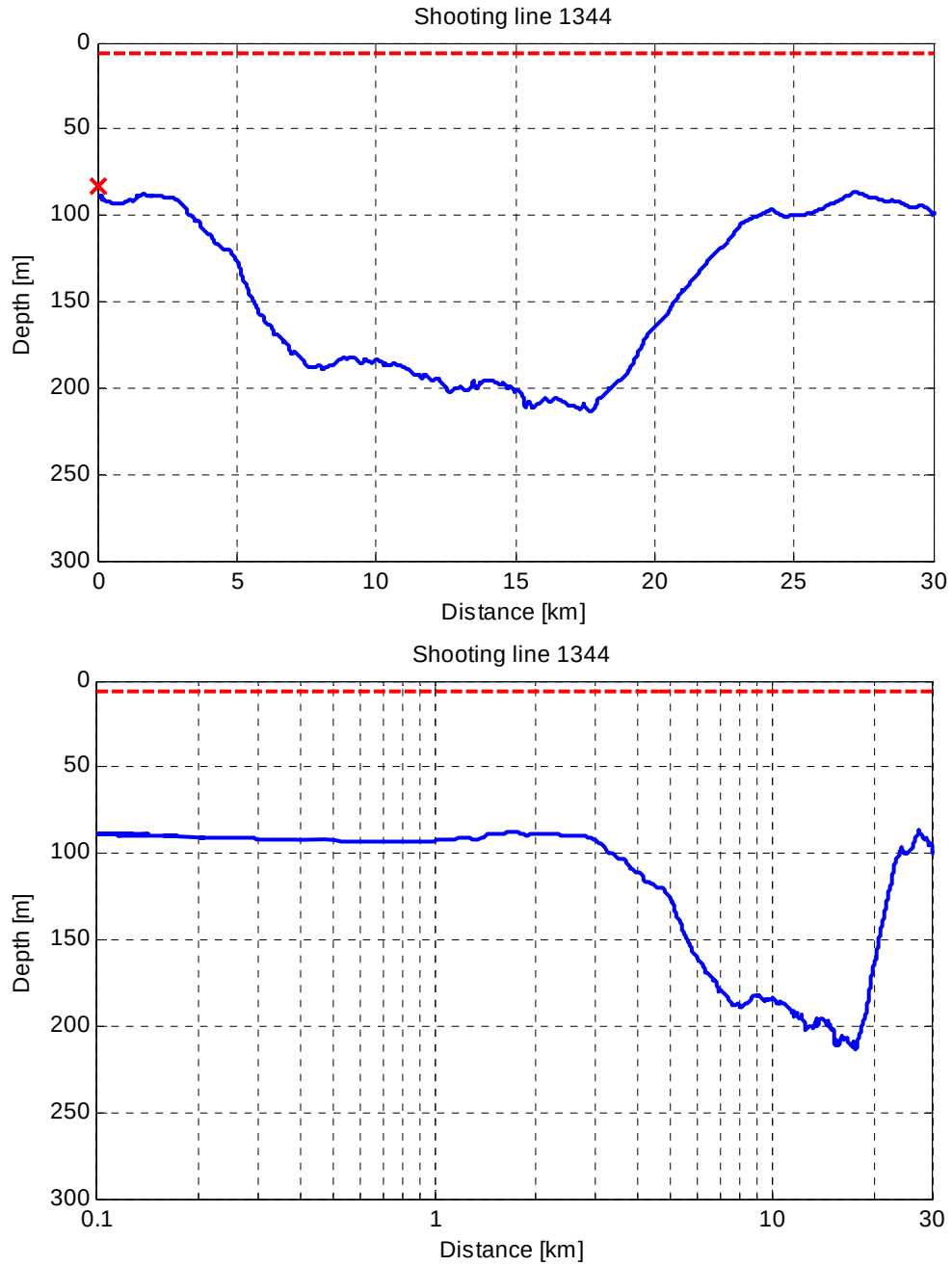

Figure 3 **Depth along shooting line 1344. Depth data from the log file of the vessel "Geo Pacific". The red cross is the placement of the receiver, and the red dashed line is the towing line. Upper: Linear x-axis. Lower: Logarithmic x-axis.**

The depth directly below the vessel can be seen in Figure 3. The depth profile is shown with both linear and logarithmic representation of the distance from the receiver. Logarithmic representation makes it easier to compare the depth profile with the sound exposure level (SEL) and the peak pressure level (PPL) which is illustrated with logarithmic x-axis.

2.3 Sound Speed Profile

The Institute of Marine Research did several measurements of the CTD (Conductivity, Temperature and Depth) of the water during the survey. From CTD one can extract sound speeds as a function of depth (a sound speed profile). The measurements were done at different locations at different time. In Figure 4 the

different sound speed profiles can be seen together with the location of each profile. The time of collection where the 23rd (red line), 26th (green line), 28th (purple line), and 30th (blue line) of June 2009. The recordings of shooting line 1344 were done at the 8th and 9th of July, but since the sound speed profiles collected close to these dates were collected at completely different locations, they were not used. It is therefore assumed that the sound speed profiles did not change much during the time from the 23rd of June to the 8th and 9th of July.

As can be seen in Figure 4 the different sound speed profiles differ according to their location. They do, however, have the same tendency of a local minimum in the sound speed at approximately 50 m depth.

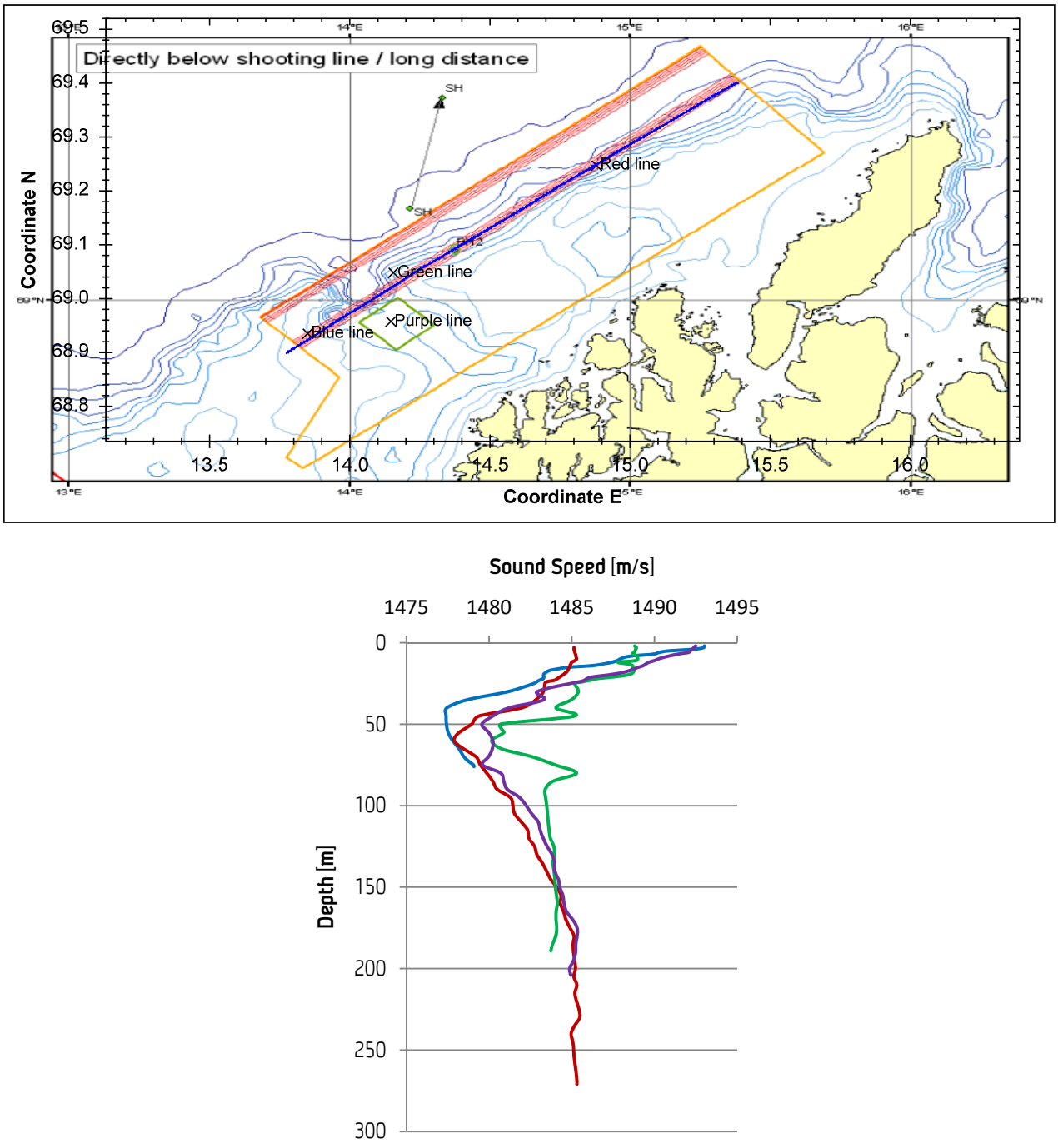

Figure 4 **Sound speed measurements from Nordland VII. Above: Illustration of where the sound speed profiles where collected. The names correspond to the sound speed profiles with the specified color in the lower plot. Lower: Sound speed profiles collected. Colors correspond to the names in the upper plot.**

To find the sound speed profile to be used in PlaneRay the average of the four selected profiles where calculated. The average can be seen in Figure 5.

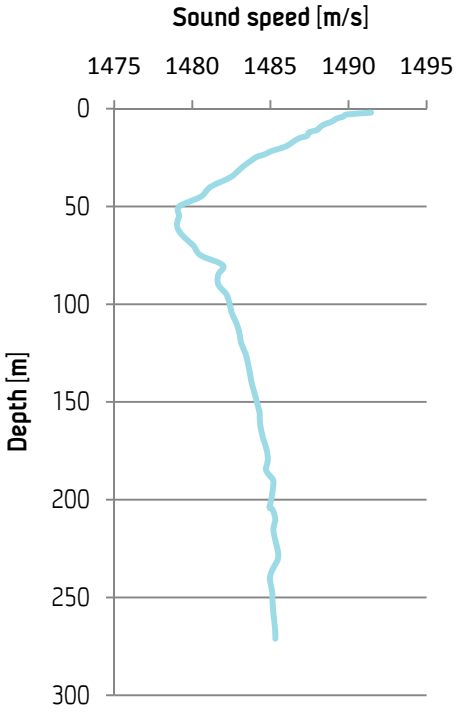

Figure 5 **Plot of the sound speed profile used in the PlaneRay model. The sound speed profile is an average of four profiles collected during the seismic survey.**

2.4 Bottom Surface

We received data of the bottom surface for the region in the survey from NGU (Geological Survey of Norway). In Table 1 the grade scale used in the classification is shown. The sediment classification of the test range can be seen in Figure 6.

Table 1 **Table showing the grade scale used in the sediment classification [2] and the density for the same sediments [3][1].**

Name	Diameter (mm)	Density (kg/m^3)
Clay	<0.002	≈ 1480
Silt	0.002 – 0.063	≈ 1740
Sand	0.063 – 2.0	≈ 2000
Gravel	2.0 – 64	-[2]
Cobble	64 – 256	-[2]
Boulder	>256	-[2]

[1] The densities are approximations from the document since the grain size partitions are different from the ones used by Hamilton.

[2] Hamilton's values do not include grain sizes above 1 mm.

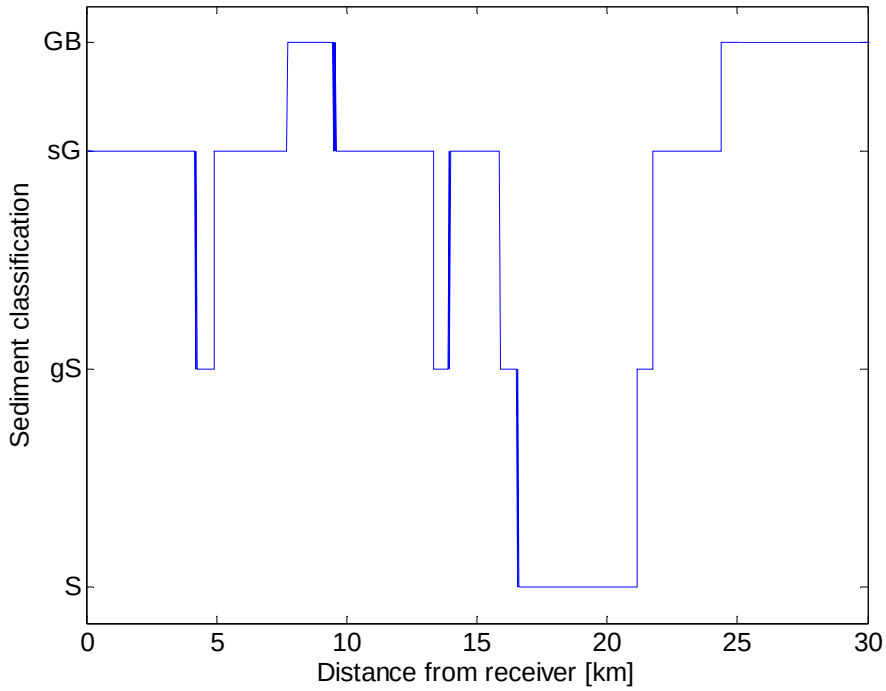

Figure 6 **Illustration of bottom sediment classification along shooting line 1344. Description of labels: S: Sand>90%, clay+silt content<10%, gravel content<2%; gS: Gravelly sand, Sand:silt+clay>9:1, gravel content<30%; sG: Sandy gravel, Sand:silt+clay>9:1, gravel content 30-80%; GB: Dominating grain sizes are gravel, cobbles and boulders. See Table 1 for the grade scale used in the classification. Sediment classification from [2].**

From the illustration of the bottom sediment in Figure 6 we can see that most of the ground consists of gravel in some sort, but there are also softer parts with mainly sand and harder parts with cobbles and boulders.

3 Measuring Results from Vesterålen

As mentioned the Institute of Marine Research measured the acoustic impulses of the shootings in the survey. The recordings were logged in intervals of 15 seconds, separated with 15 second breaks. For more information about the measuring setup see the report from the Institute of Marine Research [4].

The recordings were analyzed in Matlab where the sound exposure level (SEL) and the peak pressure level (PPL) were calculated as function of distance. The distance was calculated between the position of the bottom hydrophone and the vessel at the time of shooting with the following formula:

$$\begin{aligned} \mathrm{D} = \cos^{-1}[&\sin(\mathrm{lat}_{\mathrm{Source}}) \cdot \sin(\mathrm{lat}_{\mathrm{Receiver}}) \\ &+ \cos(\mathrm{lat}_{\mathrm{Source}}) \cdot \cos(\mathrm{lat}_{\mathrm{Receiver}}) \cdot \cos(\mathrm{long}_{\mathrm{Receiver}} - \mathrm{long}_{\mathrm{Source}})] \cdot R, \end{aligned} \tag{4}$$

where R is the earth's mean radius, 6371 km, and all longitudes and latitudes are in radians. The calculated distance does not include the depth of the hydrophone, but since the depth is small compared to the distance for most of the recordings, this was ignored.

3.1 Time response as function of distance

Figure 7 shows an illustration of how the time responses changes as function of distance. It also shows typical examples of the recorded acoustic impulse responses.

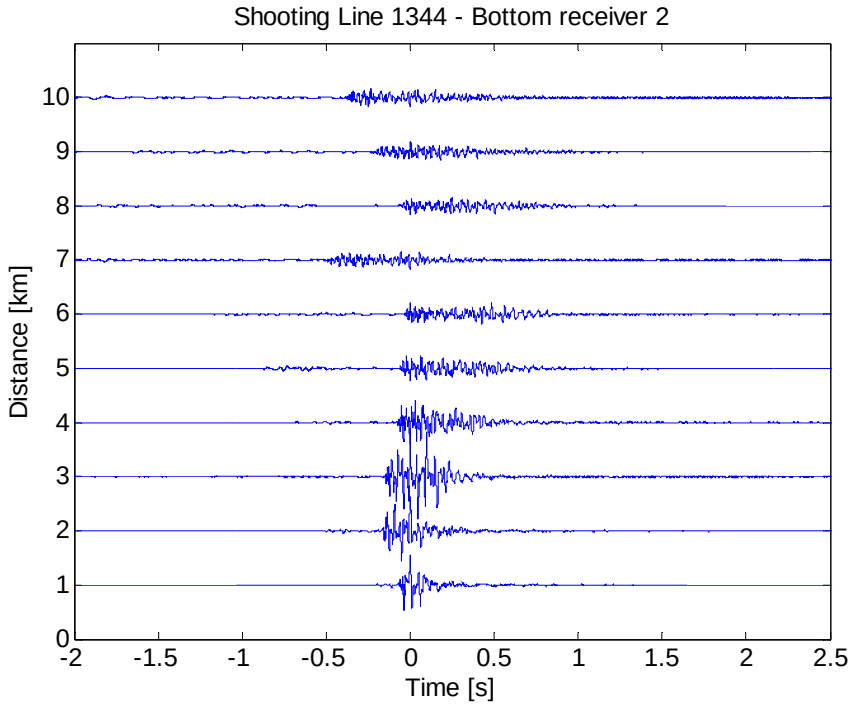

Figure 7 **Time responses as function of distance. The responses are aligned by their maximum peak value and multiplied by the distance to compensate for spherical spreading. Evidently the alignment was not successful for the response at 7 km. However, this has no consequence for the results or conclusions.**

3.2 Sound Exposure Level (SEL) and Peak Pressure Level (PPL)

In Figure 8 the SEL and PPL values are plotted as function of distance from the receiver. From 3 km a pronounced decrease can be found in both levels. This corresponds well with the bathymetry which also drops to a deeper area at this distance. After approximately 18 km the opposite can be seen – the values suddenly increases. The same happens with the bathymetry at this distance (see Figure 3).

Thus the effect of the bathymetry is significant

One may also see that the SEL follows cylindrical spreading, *-10 log(r)*, in the range where the depth is almost constant. The PPL follows *spherical spreading*, i.e. *-20 log(r)*, in the same range.
In the range interval from 3km to 7 km where the water depth increases from 100 m to 200 m the SEL and The PPL levels decrease with *40 log(r).* This behavior is typical for the so called Lloyd mirror effect and is caused by destructive interference between the direct signal and the sea surface reflected signal.

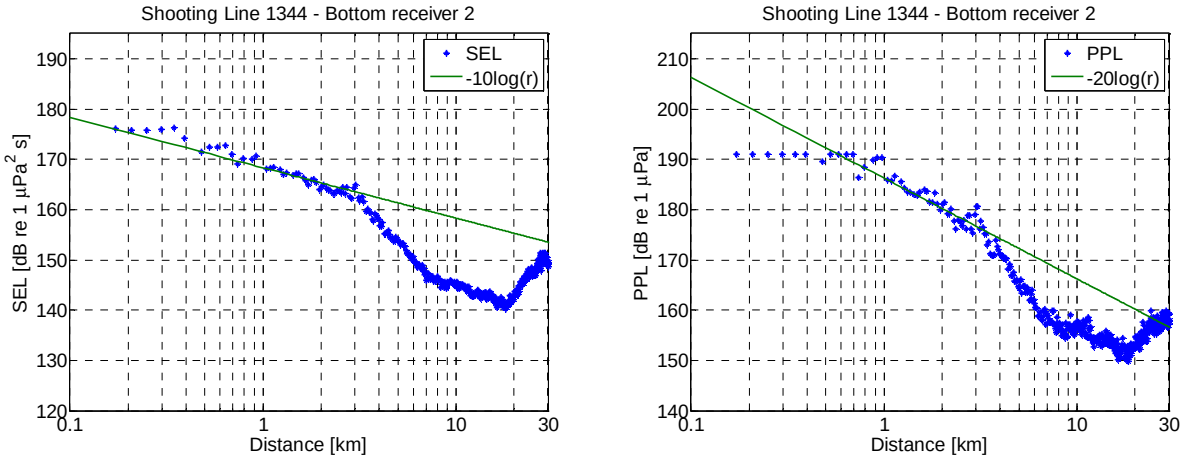

Figure 8 **Sound exposure level (left) and peak pressure level (right) from shooting line 1344 at bottom receiver 2. Left: Figure showing the SEL values found from the measured impulse responses (blue stars) and -10log(r) (green line). Right: Figure showing the PPL values found from the measured impulse responses (blue stars) and -20log(r) (green line). The signal is clipped at 191 dB, hence the distances below 1 km should be considered invalid.**

3.3 Signal Overload

The measurements are not valid below 1 km since the input signal was clipped at 191 dB. This of course affects the PPL very much. Since the peak clipped is very short in time, it does not contain much energy. Hence the SEL measurement is not affected much by the clipping. Values below 1 km should nevertheless be treated with care. In Figure 9 an example of a recording with clipped signal is shown.

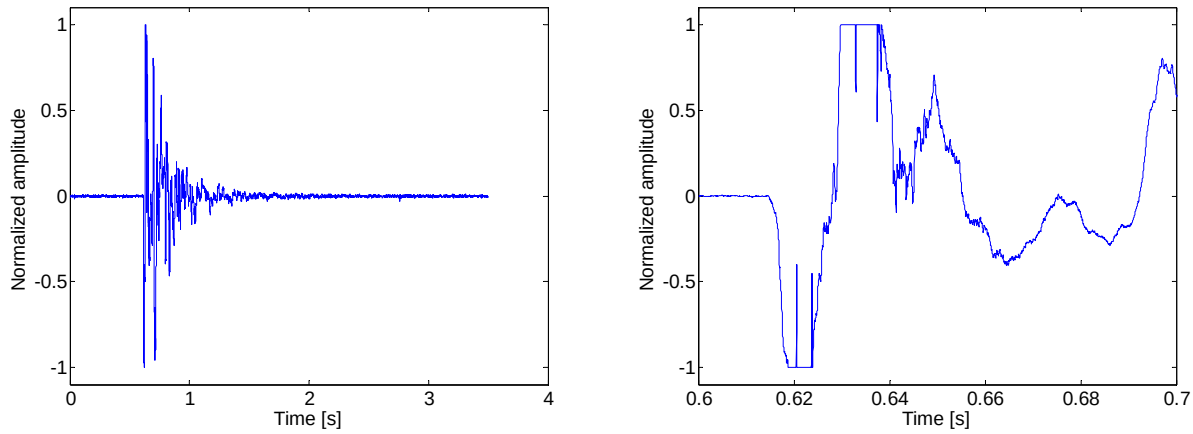

Figure 9 **Recorded signal at distance 100 meter, from shooting line 1344. The signal is clipped which is evident in the close-up look. Left: Time signal. Right: Closer look at the peak clipping.**

4 PlaneRay Model of Vesterålen

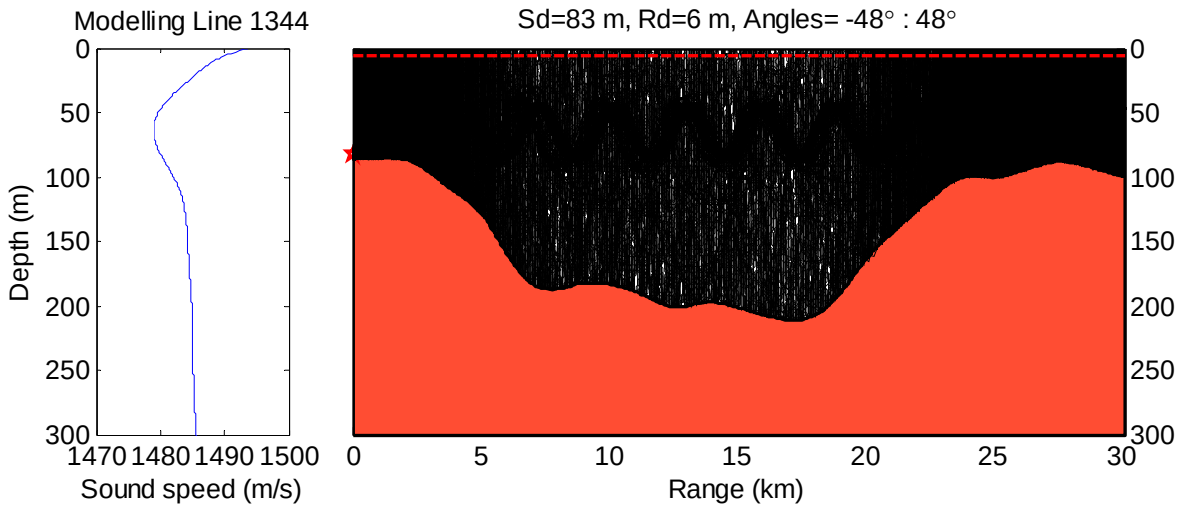

Figure 10 **Illustration of the scenario from the measurements done at line 1344 in the field Nordland VII. Left: Sound speed profile used in the model. Right: The bathymetry of the scenario. The red dotted line is the receiver line at 6 m depth, the red star is the source at 83 m and the black lines are the emanating rays from the source.**

Figure 10 shows an illustration of the model scenario. The depth profile is a smoothed (50 meter steps) version of the profile shown in Figure 3. The sound speed profile in Figure 5 is also smoothed (10 meter steps). The smoothing was applied to focus on the main properties of the profiles, not small details which might be wrong anyway due to uncertainties in the measurements.

4.1 Reciprocity

In the modeling we used the theory of reciprocity to make the computation easier. This means the source was placed on the bottom where the receiver is located in the real measurement, and vice versa (see Figure 3). The theory of reciprocity is valid as long as the source emits enough rays. See Supplement 1 for a more detailed description and a theoretical derivation of the validity.

4.2 Model Input

Important qualities of the bottom sediments when modeling with PlaneRay are:

- density of the sediment
- wave velocity (compressional and shear waves)
- attenuation (compressional and shear waves)

These qualities had to be found to be able to create a good model of the selected scenario.

The saturated bulk density of different sediment grain sizes can be seen in Figure 11 together with the compressional wave speed as function of mean grain size.

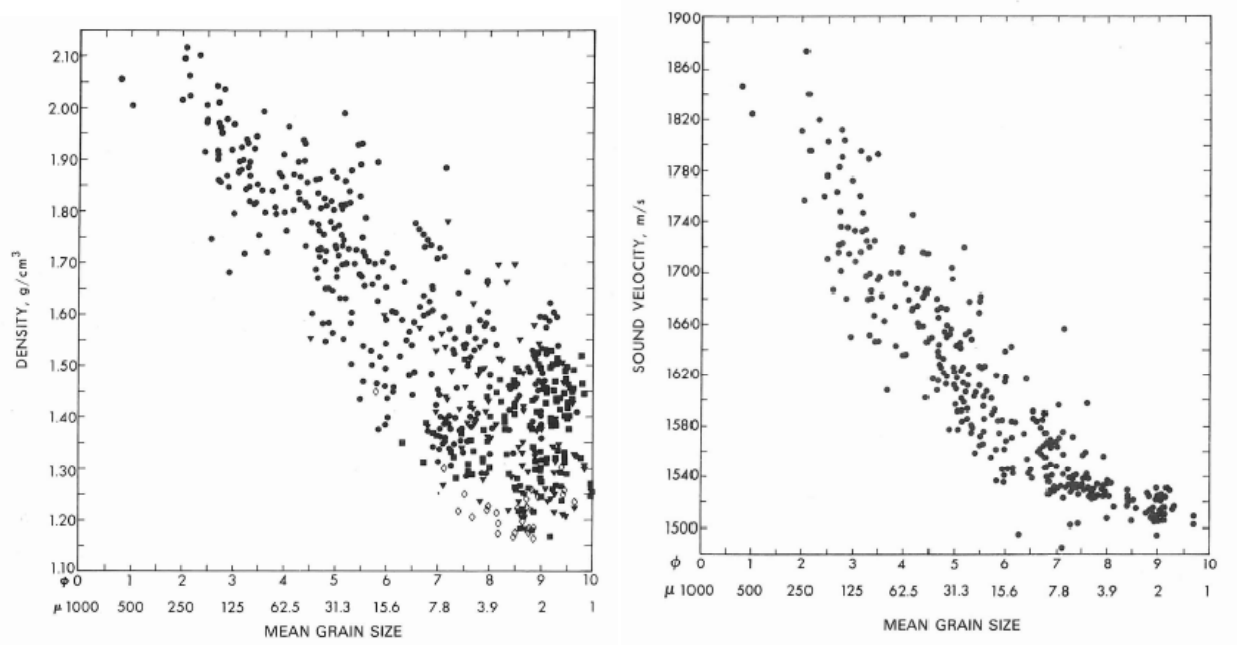

Figure 11 **Left: Mean grain size versus saturated bulk density. Right: Mean grain size versus compressional wave (sound) velocity. Figure from [3].**

The model of the scenario was created on basis of the data received. PlaneRay was fed with the smoothed versions of the mean sound speed profile (see Figure 5) and the depth profile from the research vessel (see Figure 3). The number of rays was chosen to be 100, in the angles from -48 to 48 degrees. The source depth was 83 meters and the receiver depth was 6 meters.

In Sec. 2.4 we saw that the bottom along the shooting line was mainly made of gravel in some sort. Since the model does not handle variation in sediments as function of distance we had to use the same bottom sediment for the entire range.

In Table 1 we can see that gravel is defined by NGU as grain sizes from 2 mm to 64 mm, a wide range. Since the data in Hamilton's document only includes sizes up to approximately 1 mm we had to extrapolate the results to estimate the bottom sediment properties [3]. To not move too far away from Hamilton's data, we chose to use the smallest gravel size in our model (2 mm mean grain size). Assuming that the tendency in the left plot in Figure 11 continues from 1 mm up to 2 mm, this gives a density of approximately 2 500 kg/m^3.

Extrapolating the data in the right plot in Figure 11 we find that the compressional wave speed will be approximately 2 000 m/s for a mean grain size of 2 mm.

In the same document by Hamilton we find that the attenuation is approximately 0.1 dB/ λ.

In Hamilton's document the shear wave velocity is also given as s function of compressional wave velocity. A compressional wave velocity of 2 000 m/s gives a shear wave velocity of 600 m/s. The attenuation of the shear wave was chosen to be 1 dB/ λ, estimated by the use of the first-power relationship to the frequencies given by the data in Hamilton's document.

4.2.1 Source Signal

The modeling results, especially the startle response simulations in Sec. 5.3, depend heavily on the source signal given as input. Ricker pulses are often used in seismic modeling as source signal. A Ricker pulse with centre frequency 50 Hz was used in the model (see Figure 12). To be able to compare the modeled results

with the real measurements, with regard of the amplitude value, the source was adjusted with 255 dB re µPa according to the airgun specification.

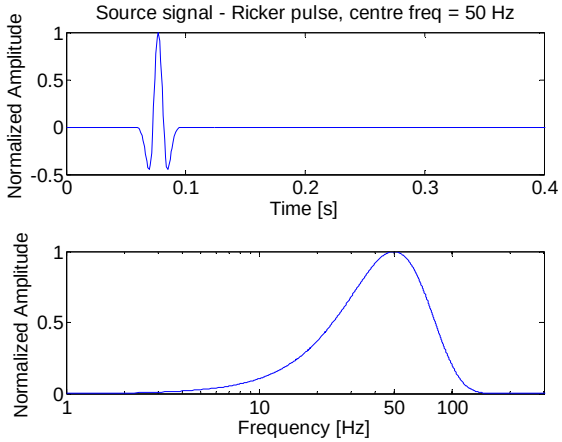

Figure 12 **Source signal used in the model. The signal is a Ricker pulse with centre frequency 50 Hz.**

PlaneRay also has the opportunity of taking into account multi sonar arrays. Multi sonar arrays for seismic surveys are optimized for a maximized constructive interference between the different sonars, in the vertical direction. This means the sonars are fired at different time and with different amplitude. Since we do not have detailed specification of the airgun used, in respect of timing and source level, this has not been included in this project. One should, nevertheless, be aware that the modeled results, especially the peak levels, might be too high due to this simplification. The multi sonar arrays are described more in detail in Supplement 2.

4.3 Modeling Results

In the following figures the SEL and PPL from the modeling results are shown. Different geo-acoustic properties of the bottom are used in the evaluation and these are given in Table 2.

Table 2 **The table shows the different parameters used in the simulations. All speeds (c_x) are in m/s, the densities (ρ_x) are kg/m^3 and the absorptions (α_x) are in dB per wavelength of the respective media. PlaneRay has the opportunity of specifying two different sediments in the bottom. This was not exploited in these simulations.**

Description	c_{p1}	c_{s2}	α_{p1}	α_{s2}	ρ_1
Original model	2 000	600	0.1	1	2 500
Hard bottom	4 000	600	0.01	1	2 600
Soft bottom	1 500	300	0.1	1	1 200
Constant sound speed	2 000	600	0.1	1	2 500
Winter sound speed profile	2 000	600	0.1	1	2 500

4.3.1 Original Model

The original model was implemented as close to the real situation as possible. Using the parameters described above the result in Figure 13 was found. As can be seen the decrease in level from 3 km to 18 km is also present in the modeled results. Approximately the same spreading in SEL and PPL, cylindrical and spherical respectively, together with -40log(r) where the depth increases, can also be seen. Thus the model seems capable to capture the significant bathymetry effect present in the measured data.

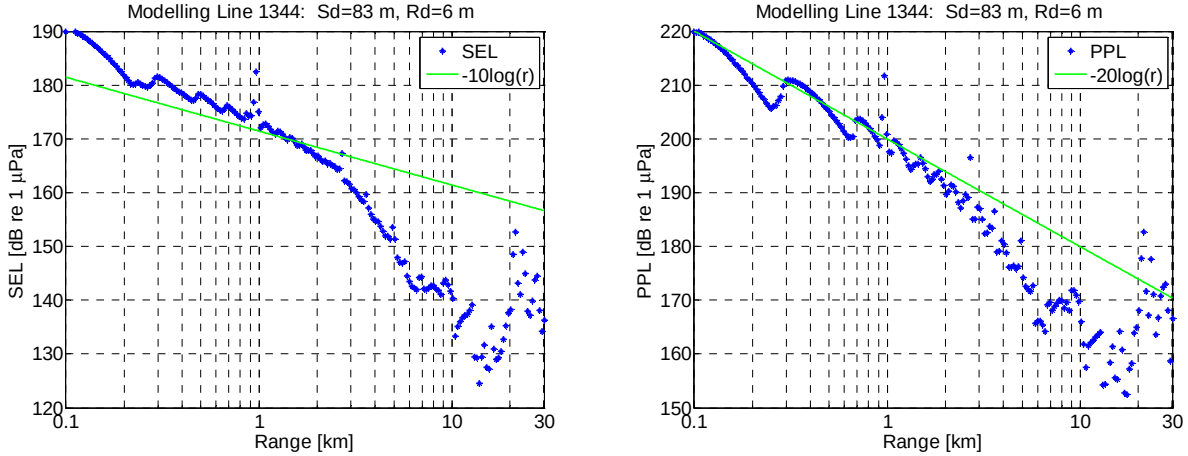

Figure 13 **Sound exposure level (left) and peak pressure level (right) calculated from the output of PlaneRay. The source is adjusted with 255 dB re µPa according to the airgun specification. Input parameters: Compressional wave speed: 2 000 m/s, bottom density: 2 500 kg/m3, compressional wave attenuation: 0.1 dB/λ, shear wave speed: 600 m/s, shear wave attenuation: 1 dB/ λ.**

4.3.2 Hard Bottom

Since the sound speed increases in the upper layers of the water the emanating rays will quickly be deflected towards the bottom. The bottom sediment could therefore have a major impact on the results. In Figure 14 the result from the hard bottom is shown. There are only small changes from the original model.

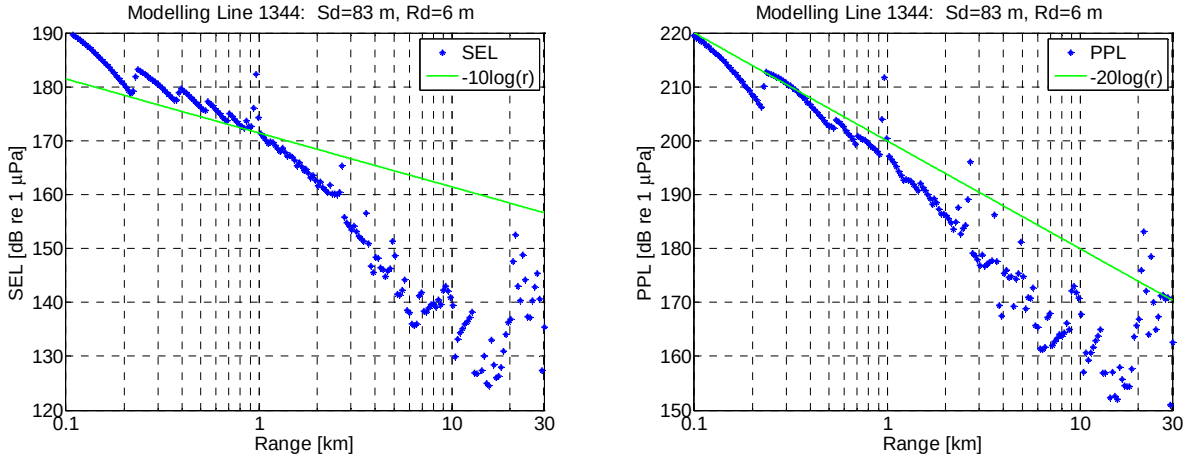

Figure 14 **Sound exposure level (left) and peak pressure level (right) calculated from the output of PlaneRay with hard bottom surface. The source is adjusted with 255 dB re µPa according to the airgun specification. Input parameters: Compressional wave speed: 4 000 m/s, bottom density: 2 600 kg/m3, compressional wave attenuation: 0.01 dB/λ, shear wave speed: 600 m/s, shear wave attenuation: 1 dB/ λ.**

4.3.3 Soft Bottom

The same modeling was done with soft bottom. In Figure 15 the results can be seen. The decrease in both SEL and PPL are even more pronounced even if there are large variations along the x-axis. This shows that the softer bottom sediment has an impact on the results.

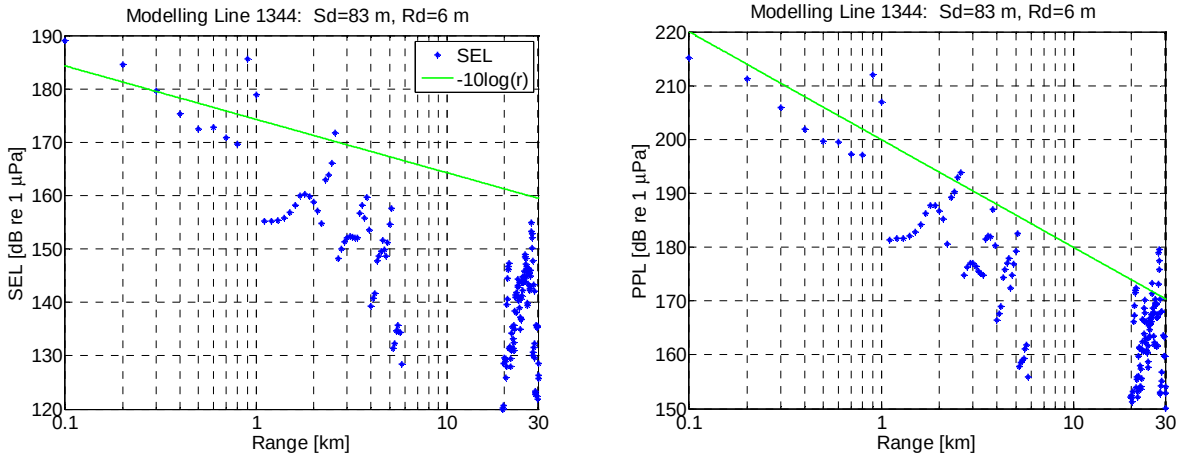

Figure 15 **Sound exposure level (left) and peak pressure level (right) calculated from the output of PlaneRay with soft bottom surface. The source is adjusted with 255 dB re µPa according to the airgun specification. Input parameters: Compressional wave speed: 1 500 m/s, wave attenuation: 0.1 dB/, and bottom density: 1 200 kg/m^3. The shear speed is zero.**

4.3.4 Constant Sound Speed

The model was also run with constant sound speed (1 495 m/s). Figure 16 shows the results. As can be seen the 3-18 km dip is reduced. Just above 10 km there is also an increase in both the SEL and PPL values, due to reflections from the bottom around the source.

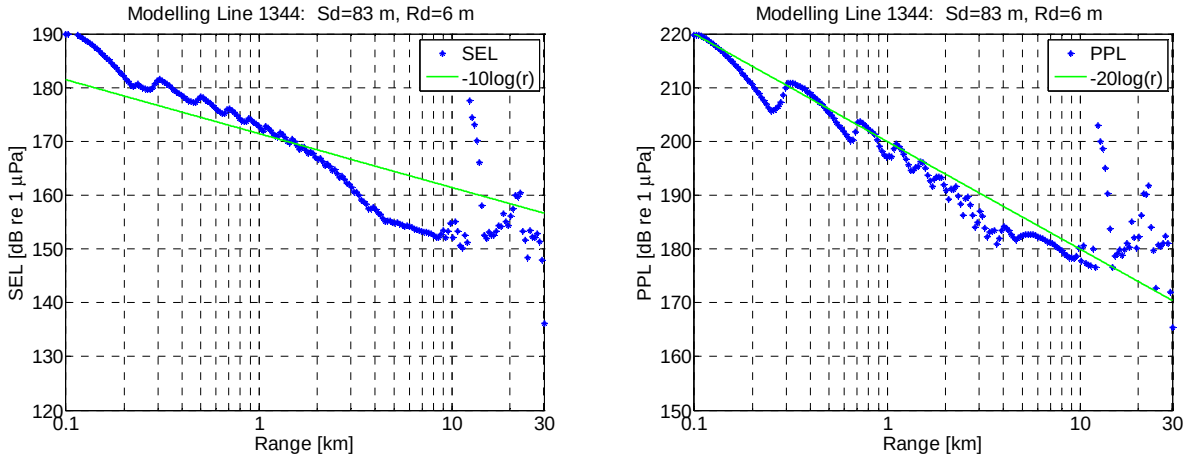

Figure 16 **Sound exposure level (left) and peak pressure level (right) calculated from the output of PlaneRay with constant sound speed (1 495 m/s). The source is adjusted with 255 dB re µPa according to the airgun specification. Input parameters: Compressional wave speed: 2 000 m/s, bottom density: 2 500 kg/m3, compressional wave attenuation: 0.01 dB/λ, shear wave speed: 600 m/s, shear wave attenuation: 1 dB/ λ.**

4.3.5 Winter Sound Speed Profile

A typical winter sound speed profile was also used with the same bathymetry. This was done to see if there were large differences in results if the seismic survey had been done at a different time of the year. The sound speed profile used is from the Halten Bank and is the same winter profile used later in Sec. 6 where different seasonal sound speed profiles are compared. Because of the cold temperature above the surface during the winter, the sound speed decreases as you move towards the upper layers of the water.

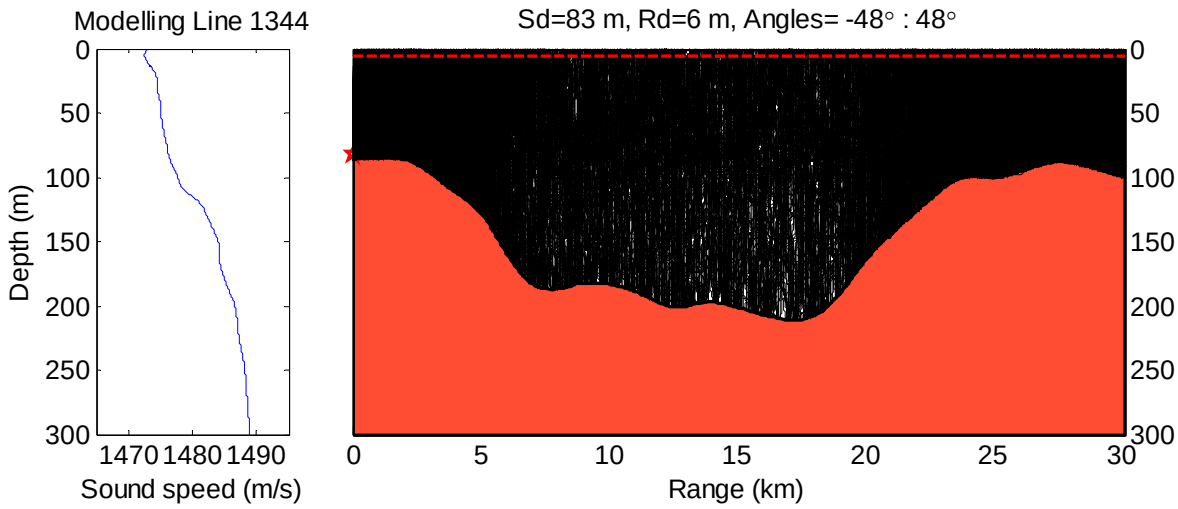

Figure 17 **Illustration of the winter model setup. Left: Typical winter sound speed profile. Right: The bathymetry of the scenario. The red dotted line is the receiver line at 6 m depth, the red star is the source at 83 m and the black lines are the emanating rays from the source.**

In Figure 18 the SEL and PPL levels can be seen. It can be seen that there are large variations in both SEL and PPL above 5 km. This is due to the sound channel created in the upper layer of the sea. The positive gradient of the sound speed profile makes the sound waves bend upwards to the surface creating caustics, or hot-spots as they often are called. Caustics are a common phenomenon in underwater acoustic propagation and will locally create large peaks. The locations of these areas are not stable meaning they are very sensitive to small variations in oceanographic conditions.

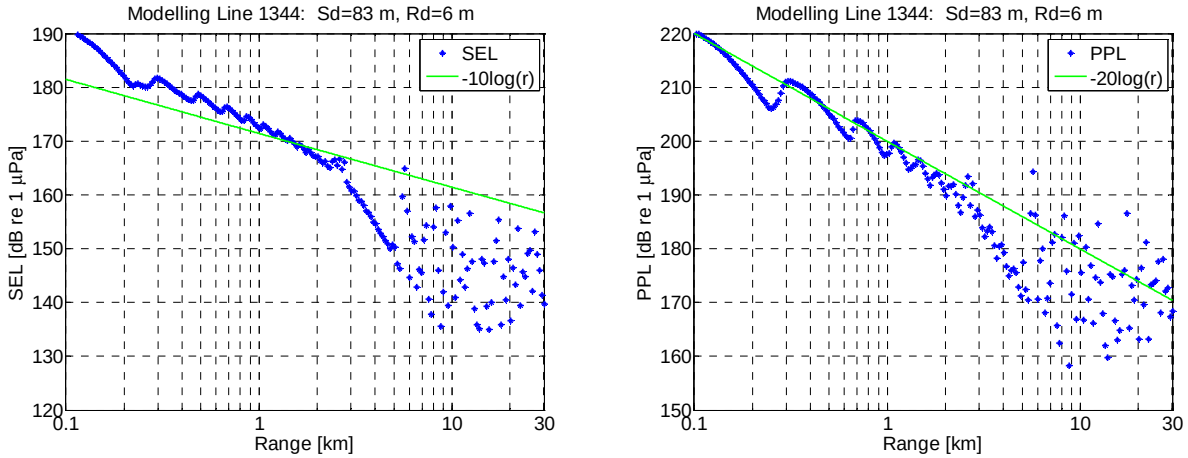

Figure 18 **Sound exposure level (SEL) and peak pressure level (PPL) for the line 1344 with winter sound speed profile. Input parameters: Compressional wave speed: 2 000 m/s, bottom density: 2 500 kg/m3, compressional wave attenuation: 0.1 dB/λ, shear wave speed: 600 m/s, shear wave attenuation: 1 dB/ λ.**

5 Startle Reaction – Cod

The University of Oslo has measured startle threshold for cod. They have studied the behavior of fish in a small water tank while exposing them to sound. In Table 3 and Figure 19 the threshold values can be seen. The values are preliminary and might be changed in the final report from the University of Oslo.

Table 3 Startle threshold levels for cod. Measurements are done by the University of Oslo.

Frequency [Hz]	Peak amplitude [dB re 1 µPa]
10	> 173
30	171
70	162
100	160
160	157
320	169

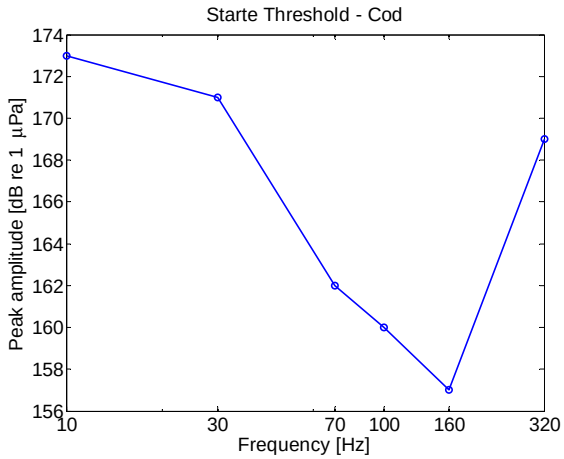

Figure 19 Plot of startle thresholds as a function of frequency.

The results from both the measurements and the modeling were transferred to the frequency domain and compared to the startle thresholds for cod. Distances from 0.1 km to 30 km were used. The results are shown in a contour plot with frequency and range as the y- and x-axis, respectively.

5.1 Critical Range

The longest distance where the sound exposure exceeds the threshold limit is called *critical range* from now on. Each set of parameters and scenario will have its own critical range.

5.2 Measuring Results from Vesterålen

Impulse responses at different distances where selected and transferred to the frequency domain. Discrete Fourier Transform (DFT) was used with *N=10*Fs*. *Fs* were 48 000 Hz. Figure 20 displays the area, in range and frequency, where the sound exposure level exceeds the startle threshold values for cod shown in Figure 19 and given in Table 3. The startle level is exceeded for all frequencies in the range from 10 Hz to 180 Hz with the largest extensions out to 5 km for frequencies around 50 Hz. In addition, the threshold is exceeded for ranges beyond 24 km due to the increased sound level caused by the change in water depth in that range interval. Therefore the critical range for the measured impulse responses is found to be 30 km, but it must be noted that the threshold limit is exceeded by only 1 – 2 dB above 24 km.

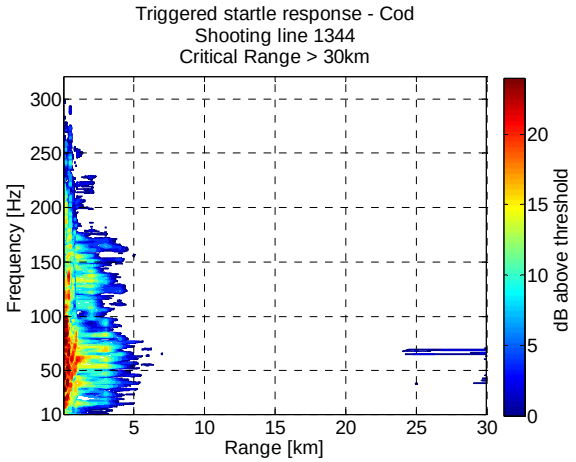

Figure 20 **Plot of the triggered startle response for cod from the measured results done at Nordland VII, shooting line 1344.**

5.3 Modeling Results from Vesterålen

The same frequency analysis where done on the modeled results. In the following figures the same scenarios as described in Sec. 4.3 are shown.

5.3.1 Original Model

The original model gives the result shown in Figure 21. It is obvious that the source signal used is missing some frequency components, especially above 100 Hz. The frequency range from 10 to 100 Hz is, however, similar as the measured responses, and this region is also the one propagating furthest. The critical range is 5 km. This is in good agreement with the observed except that the modeled result does not detect the values around 24km to 30 km.

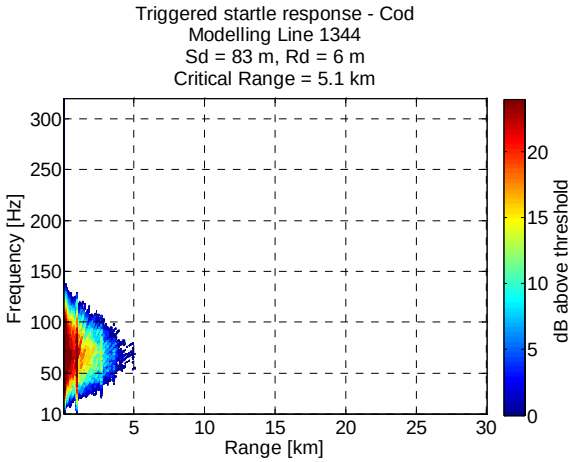

Figure 21 **Plot of the triggered startle response from the modeled results of shooting line 1344 at Nordland VII. Input parameters: Compressional wave speed: 2 000 m/s, bottom density: 2 500 kg/m3, compressional wave attenuation: 0.1 dB/λ, shear wave speed: 600 m/s, shear wave attenuation: 1 dB/ λ.**

In order to test the sensitivity of the model the analysis was repeated with a 20 dB reduction in threshold level. Figure 22 shows that the modeled result now gives an area starting just above 20 km. However, in this range the original threshold is exceeded with only 1-2 dB, which indicates that sensitivity to small changes in threshold values or in sound level assessment is of crucial importance for the determination of critical range.

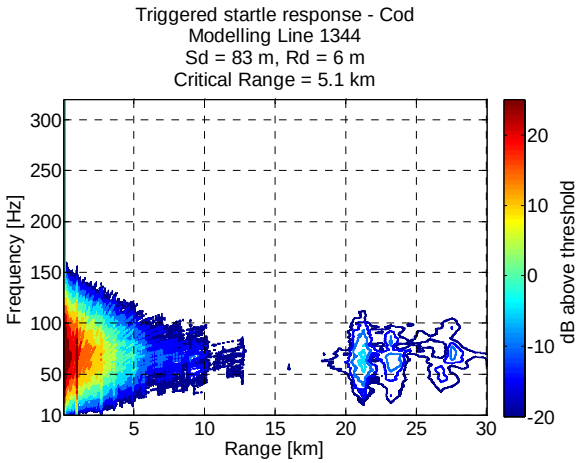

Figure 22 **Plot of the triggered startle response, with lower threshold limit (20 dB below the original one) to see if the modeled result also has a reoccurring area around 25 km, as the real measurement.**

5.3.2 Hard Bottom

In Figure 23 the results from the hard bottom can be seen. The result shows that the levels go below the threshold limit earlier than the original model.

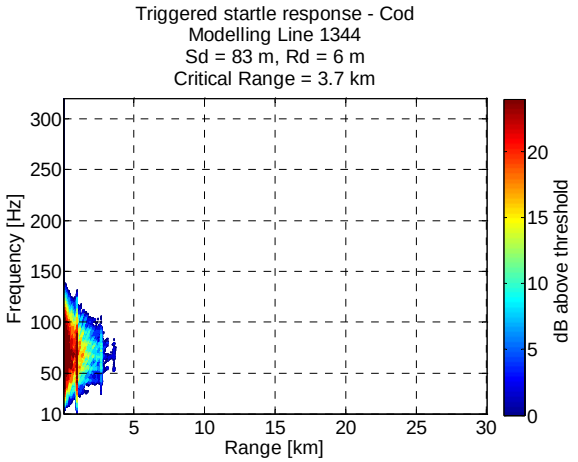

Figure 23 **Plot of the triggered startle response from the modeled results of shooting line 1344 at Nordland VII. Input parameters: Compressional wave speed: 4 000 m/s, bottom density: 2 600 kg/m3, compressional wave attenuation: 0.01 dB/λ, shear wave speed: 600 m/s, shear wave attenuation: 1 dB/ λ.**

5.3.3 Soft Bottom

The results from the model run with soft bottom can be seen in Figure 24. Keeping the results in Sec. 4.3.3 in mind, it is no surprise that the triggered startle response goes below the threshold even earlier than both the original and the hard bottom model.

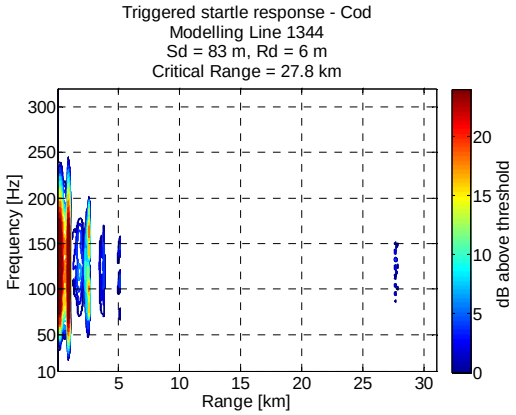

Figure 24 **Plot of the triggered startle response from the modeled results of shooting line 1344 at Nordland VII using soft bottom parameters. Input parameters: Compressional wave speed: 1 500 m/s, bottom density: 1 200 kg/m3, compressional wave attenuation: 0.1 dB/λ, zero speed and shear wave attenuation.**

5.3.4 Constant Sound Speed

The evaluation of the constant sound speed (1495 m/s) gives the triggered startle response curves in Figure 25. It is possible to see that the startle threshold is exceeded at a much longer distance. The large increase around 13 km is due to a bottom reflection which does not reach the receiver in the original model. The critical range is 25.3 km.

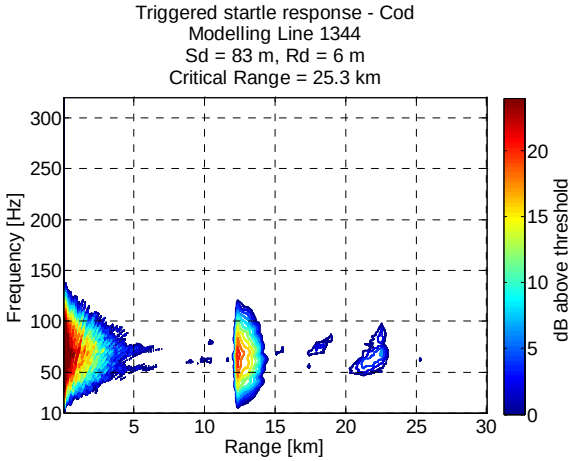

Figure 25 **Plot of the triggered startle response from the modeled results of shooting line 1344 at Nordland VII using constant sound speed. Input parameters: Compressional wave speed: 2 000 m/s, bottom density: 2 500 kg/m3, compressional wave attenuation: 0.1 dB/λ, shear wave speed: 600 m/s, shear wave attenuation: 1 dB/ λ.**

5.3.5 Winter Sound Speed Profile

The winter sound speed profile gives the results shown in Figure 26. Because of the same hot-spot effect mentioned in Sec. 4.3.5, we get local maximum values exceeding the threshold further out than the original model. This increase gives a critical range of 12.3 km.

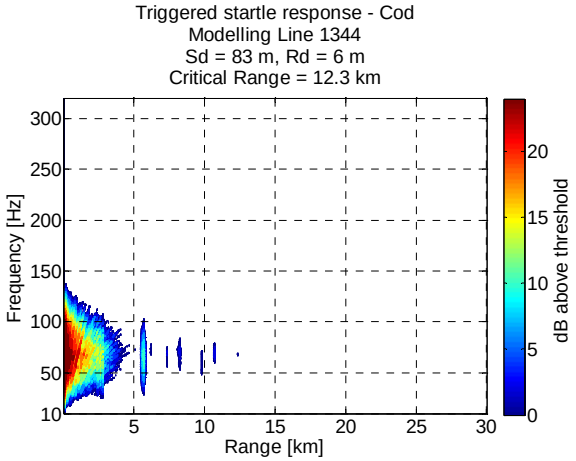

Figure 26 **Plot of the triggered startle response from the modeled results of shooting line 1344 at Nordland VII using winter sound speed profile. Input parameters: Compressional wave speed: 2 000 m/s, bottom density: 2 500 kg/m3, compressional wave attenuation: 0.1 dB/λ, shear wave speed: 600 m/s, shear wave attenuation: 1 dB/ λ.**

6 PlaneRay Model of the Halten Bank

Because of the seasonal effect seen in the above results we decided to examine how the change in sound speed profile affects the results. The following section therefore evaluates the effects of seasonal variations in the oceanographic conditions. The Halten Bank area is selected for the evaluation because of its interest for seismic surveys and also because oceanographic data is easy available for this area. To only focus on the seasonal effect the bathymetry is kept constant flat, which also is close to how the bathymetry is at the Halten Bank. The depth of each run is determined by the depth of the collected sound speed profile.

6.1 Sound Speed Profiles

From the data made available by Norsk Marint Datasenter (NMD) in Bergen, four sound speed profiles have been selected and these sound speed profiles are shown in Figure 27 where the titles give dates and positions.

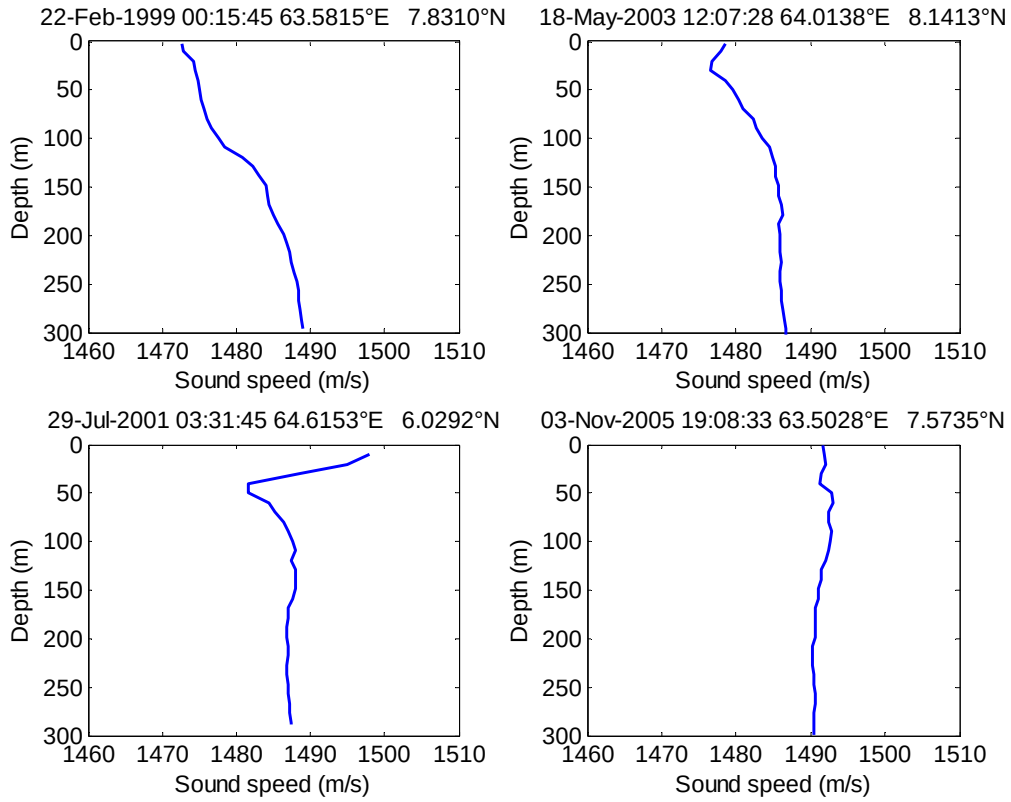

Figure 27 **Selected sound speed profiles for the Halten Bank for the study of seasonal variations. Data provided by Norsk Marint Datasenter (NMD), Bergen.**

6.2 Winter Conditions

Under typically winter conditions the sound speed increases almost monotonically with depth due to colder water near the surface and the depth effect on the sound speed. Generally, this creates a sound channel near the surface with low transmission loss to positions near the sea surface. All propagation paths to receivers close to the bottom are reflected from the bottom. Consequently, propagation to receivers close to the bottom depends strongly on the bottom reflection loss, which again depends on the geo-acoustic properties and the roughness of the bottom

These observations are demonstrated by the example with conditions at the Halten Bank in February 1999. Figure 28 shows the ray traces from a source at 8 meter depth and Figure 29 shows the channel impulse responses as function of distance from the source for the two cases of receivers at shallow depths, 25 m

depth, and at receivers 25 m above the bottom. The amplitudes in these plots are on an arbitrary relative scale. The figures show that at shallow depths, there are strong contributions from surface reflected and refracted arrivals. These are completely missing for receivers close to the bottom where all the arrivals are reflected ones or several times from the bottom.

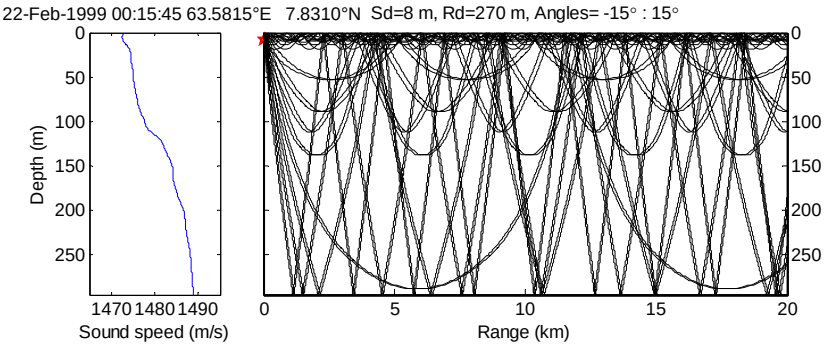

Figure 28 **Ray traces from a source at 8 m depth with a February sound speed profile.**

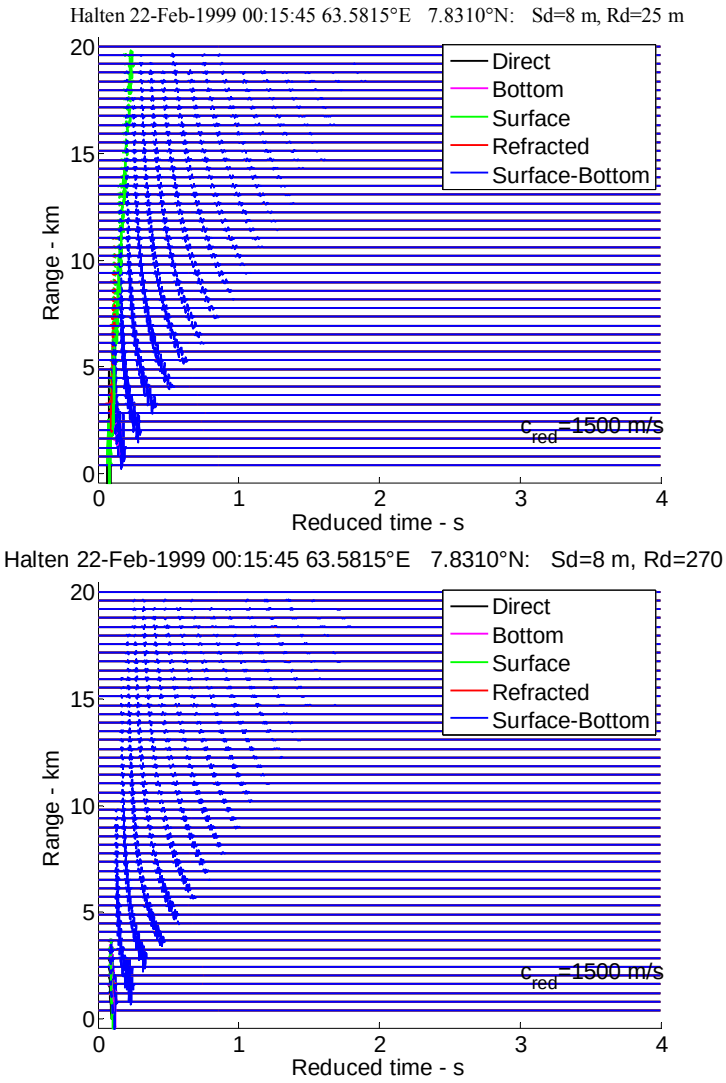

Figure 29 **Channel impulse response as function of ranges out to 20 km. Above: Receiver at 25 m depth, Below: Receiver at 270 m, 25 m above the bottom.**

Figure 30 shows the SEL and PPL as function of range for both the shallow and deep receiver. These values are calculate by integrating over the time response shown in Figure 29 scaled up by applying a source level of 255 dB rel. 1 µPa.

Notice the especially high levels for the shallow receiver at the some of the distances above 3 km. These high levels are caused by the same mechanism described in Sec. 4.3.5, called caustics or hot spots. This can also be observed in the ray traces in Figure 28. The signals at the deep receiver do not exhibit such high levels.

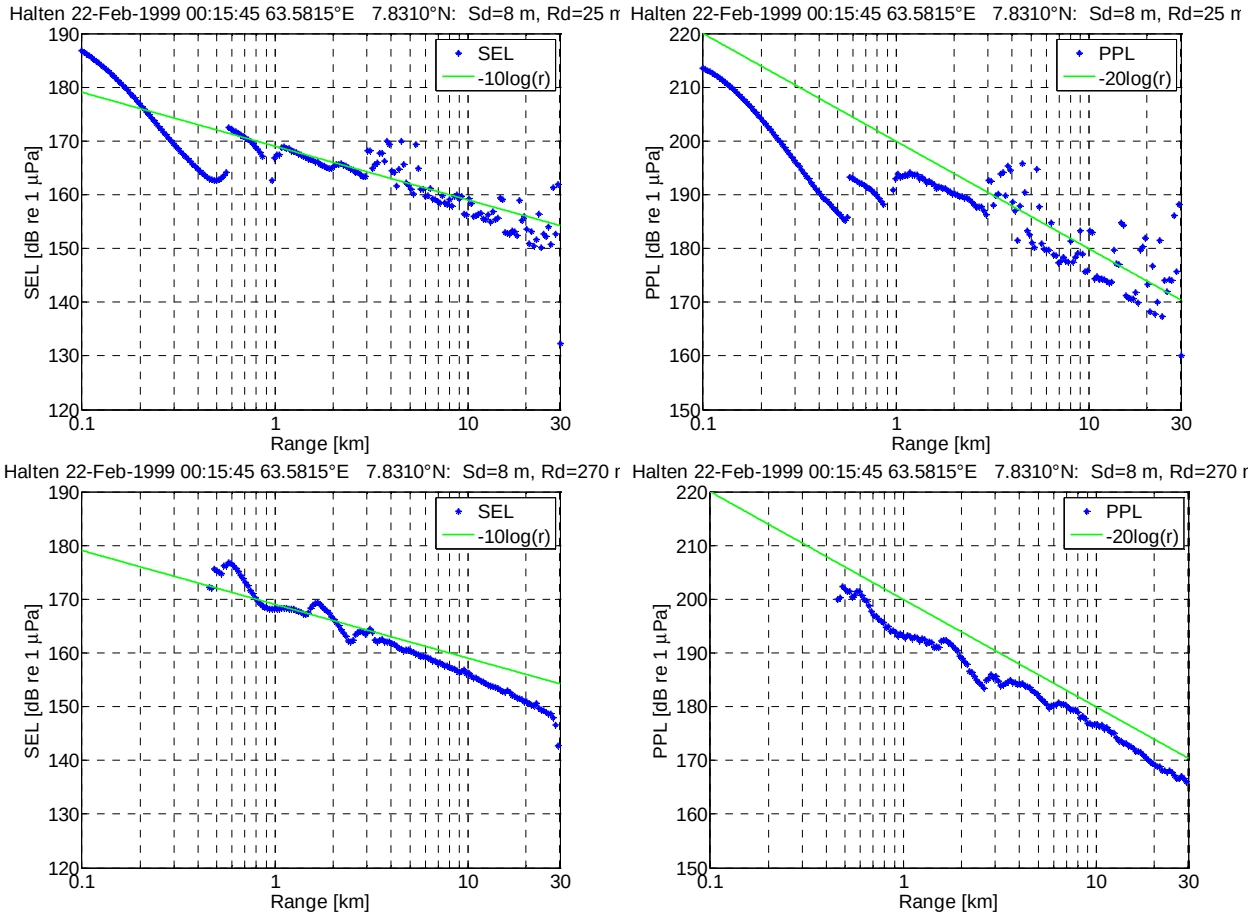

Figure 30 **Sound exposure level (SEL) and peak pressure level (PPL) for the Halten bank winter sound speed profile. Above: Receiver at 25 m depth, Below: Receiver at 270 m, 25 m above the bottom.**

6.2.1 Startle Response – Winter

In Figure 31 the triggered startle responses for cod can be seen. The receiver close to the surface exceeds the threshold at a longer distance (29.2 km) than the bottom receiver (17.9 km). This is due to the hot spots mentioned above.

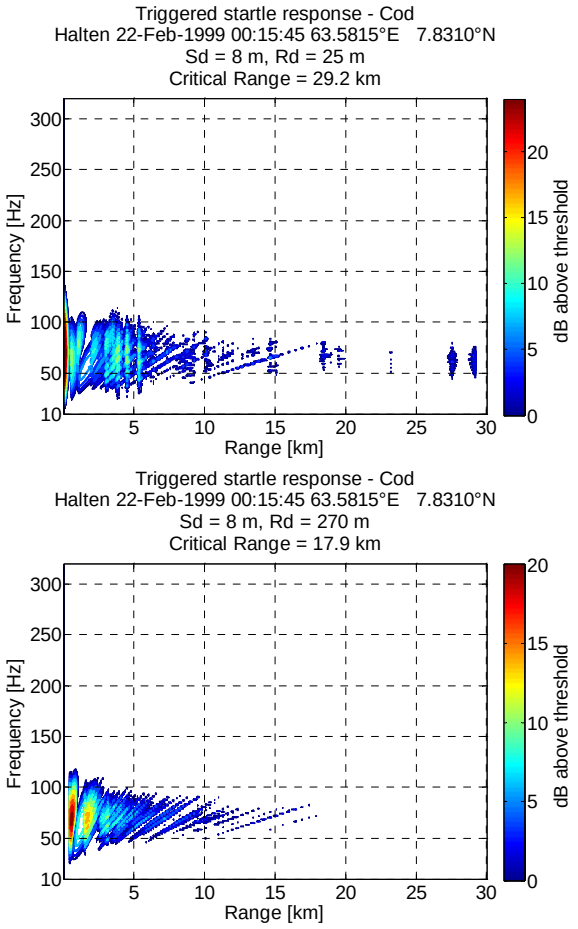

Figure 31 **Triggered startle response for the modeled result from the Halten Bank. The sound speed profile used is from February 1999. Above: Receiver at 25 m depth. Below: Receiver at 270 m, 25 m above the bottom.**

6.3 Spring

The sound speed profile for the month of May has a negative gradient near the sea surface caused by the increased surface temperature. Otherwise the profile is not very different from the February profile and the results are similar. The ray tracing results are shown in Figure 32. There is relatively strong sound cannel with axis at about 25 m, which will give relatively high sound levels at the upper part of the ocean. This is also evident from the channel impulse responses shown in Figure 33.

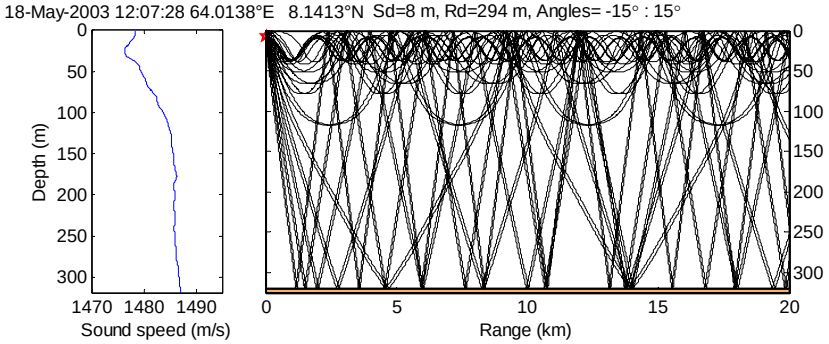

Figure 32 **Ray traces from a source at 8 m depth with a May sound speed profile.**

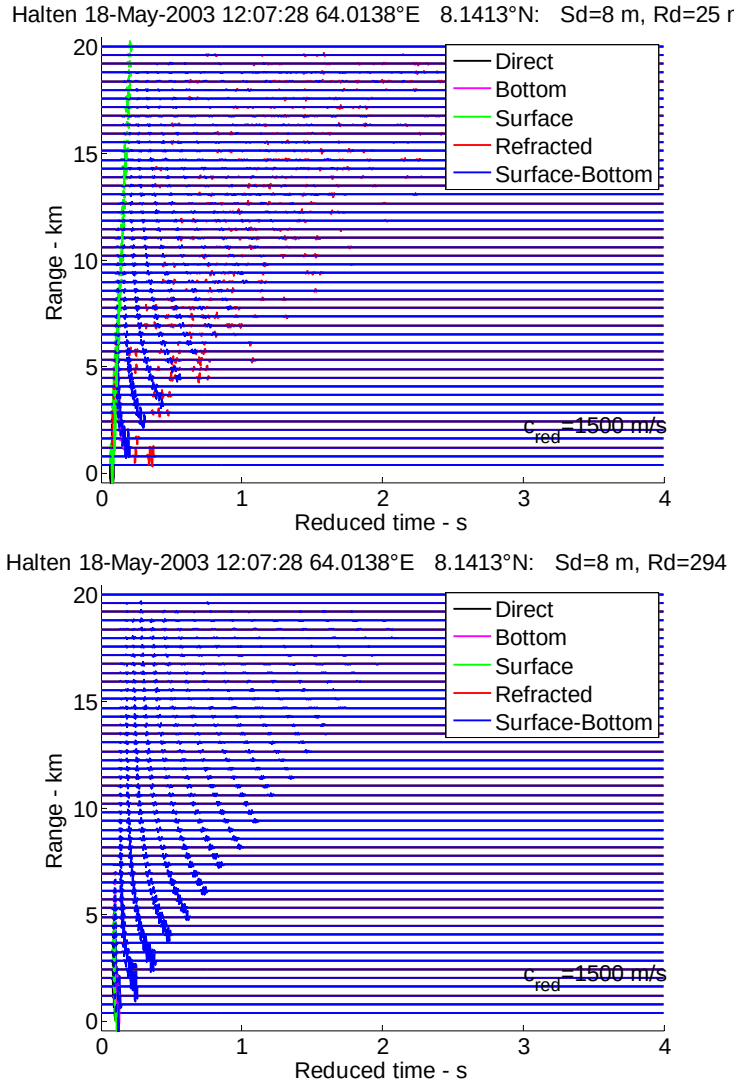

Figure 33 **Channel impulse response as function of ranges to 20 km. Above: Receiver at 25 m depth, Below: Receiver at 294 m, 25 m above the bottom.**

Figure 34 shows the SEL and PPL plotted as function of range. Most noticeable is the strong peaks in the levels for a shallow receiver, which is caused by caustics.

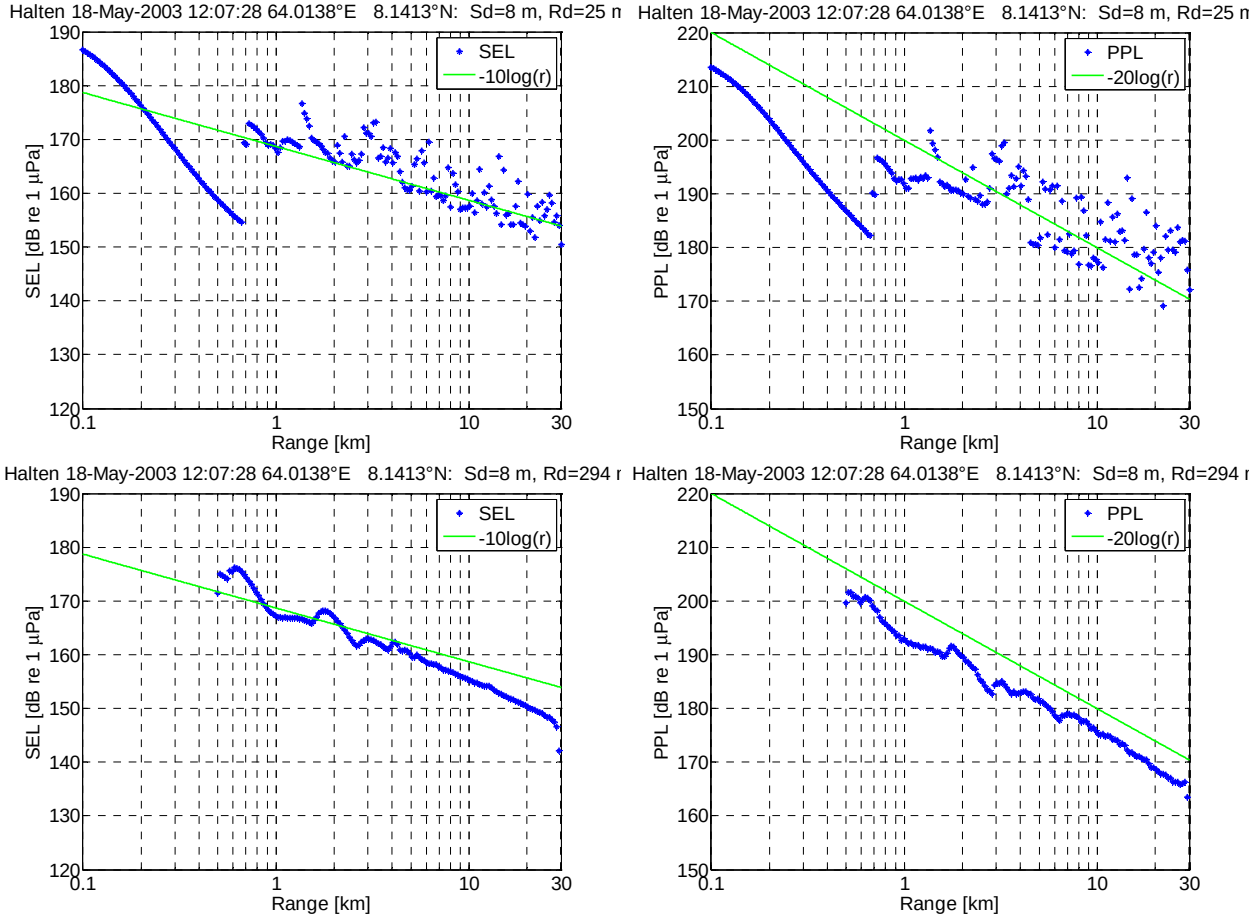

Figure 34 **Sound exposure level (SEL) and peak pressure level (PPL) for the Halten bank spring sound speed profile. Above: Receiver at 25 m depth, Below: Receiver at 294 m, 25 m above the bottom.**

6.3.1 Startle Threshold – Spring

In Figure 35 the triggered startle response for the spring sound speed profile can be seen. Also here the shallow receiver is affected by the caustics and goes above the threshold further than the receiver close to the bottom. The critical ranges are 28.3 km and 16.9 km for the shallow and deep receiver respectively.

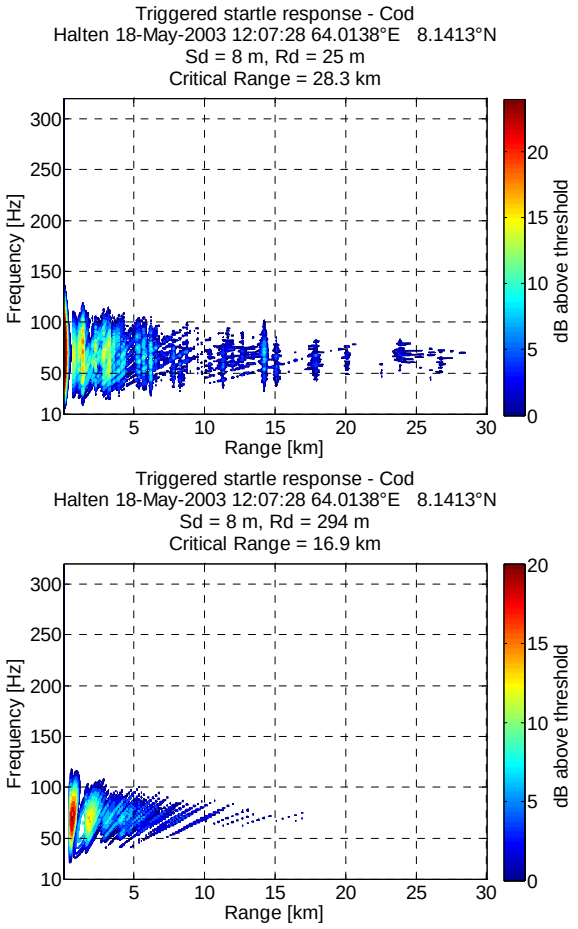

Figure 35 **Triggered startle response for the modeled result from the Halten Bank. The sound speed profile used is from May 2003. Above: Receiver at 25 m depth. Below: Receiver at 294 m, 25 m above the bottom.**

6.4 Summer

The summer profile is a July profile with a negative gradient down to a minimum sound speed at about 50 meter. This will cause a sound channel around this depth, especially if the source is located here. In our example the source is located well above this depth and therefore the sound channel is not that easy to see in Figure 36.

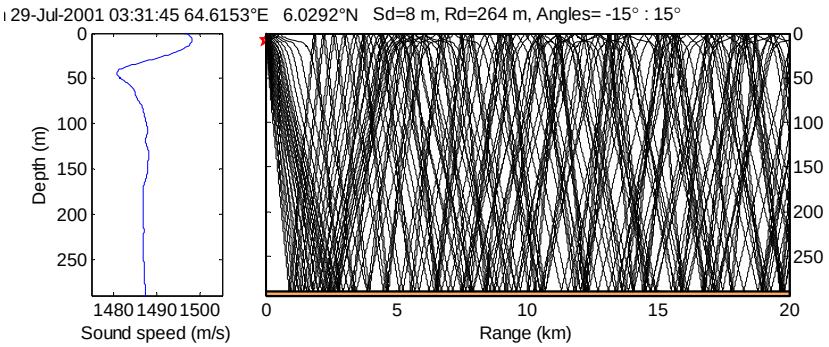

Figure 36 **Ray traces from a source at 8 m depth with a July sound speed profile.**

In Figure 37 the SEL and PPL can be seen. It is possible to see that with the summer sound speed profile there are small differences between the shallow and deep receiver. The difference at short distances are due to the modeling. Since we have limited the angle of the rays emitting to ± 30 ° no rays will reach the bottom receiver when the range is small, and the shallow receiver will only be exposed to the direct sound, no reflections. At distances above 1 km, the results are very similar.

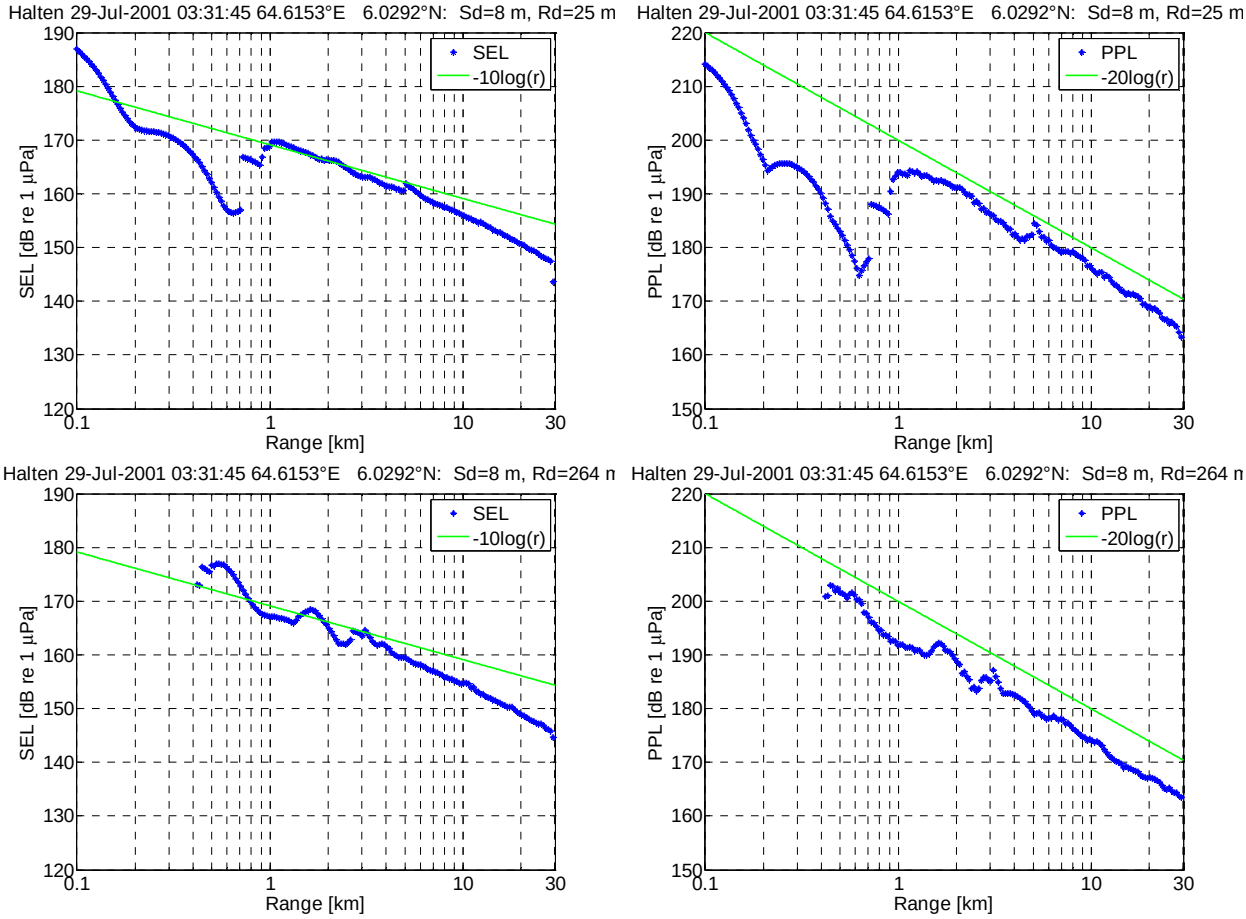

Figure 37 **Sound exposure level (SEL) and peak pressure level (PPL) for the Halten bank summer sound speed profile. Above: Receiver at 25 m depth, Below: Receiver at 264 m, 25 m above the bottom.**

6.4.1 Startle Threshold – Summer

Since both the SEL and PPL were similar for the shallow and deep receiver, it is no surprise that also the startle threshold responses are similar. For the shallow receiver the critical range is 16.9 km, and the receiver close to the bottom has a critical range of 14.2 km.

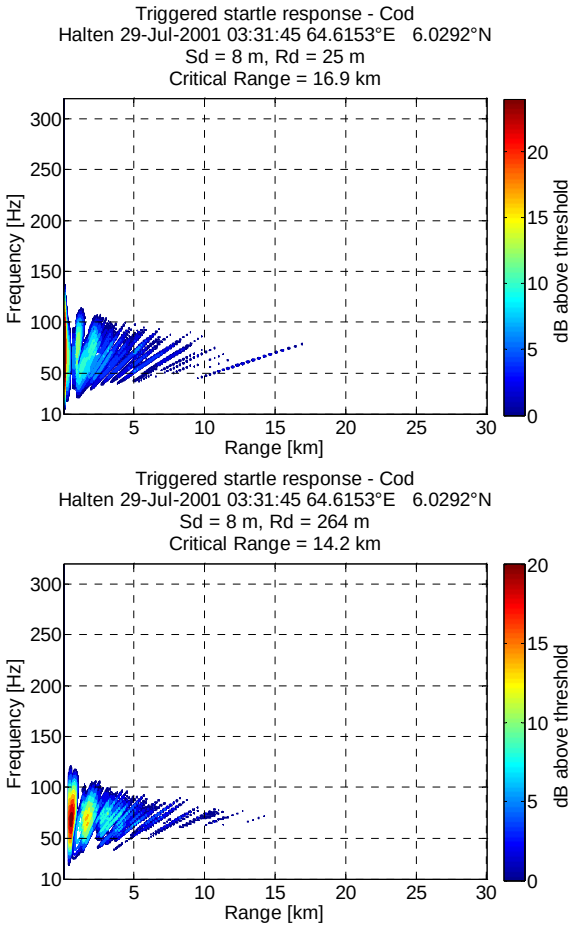

Figure 38 **Triggered startle response for the modeled result from the Halten Bank. The sound speed profile used is from July 2001. Above: Receiver at 25 m depth. Below: Receiver at 264 m, 25 m above the bottom.**

6.5 Autumn

This example of an autumn sound speed profile results in sound channel close to the sea surface extending down to approximately 50 meter, see Figure 39. In this channel there are also caustics and areas of high intensive sound, as some of the above examples.

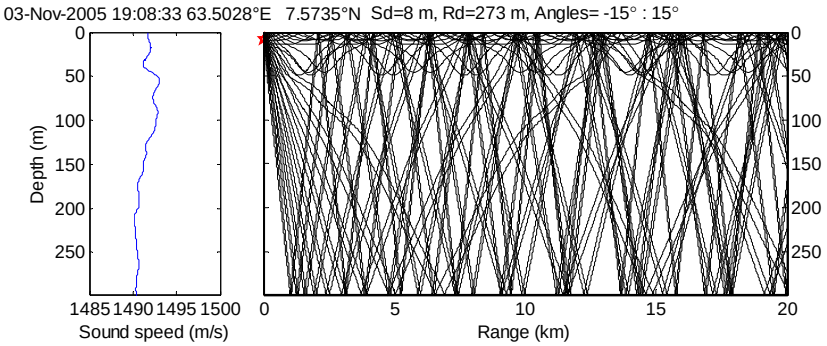

Figure 39 **Ray traces from a source at 8 m depth with a November sound speed profile.**

The same caustic effect can be seen at the shallow receiver in Figure 40. This is not present in the deep receiver.

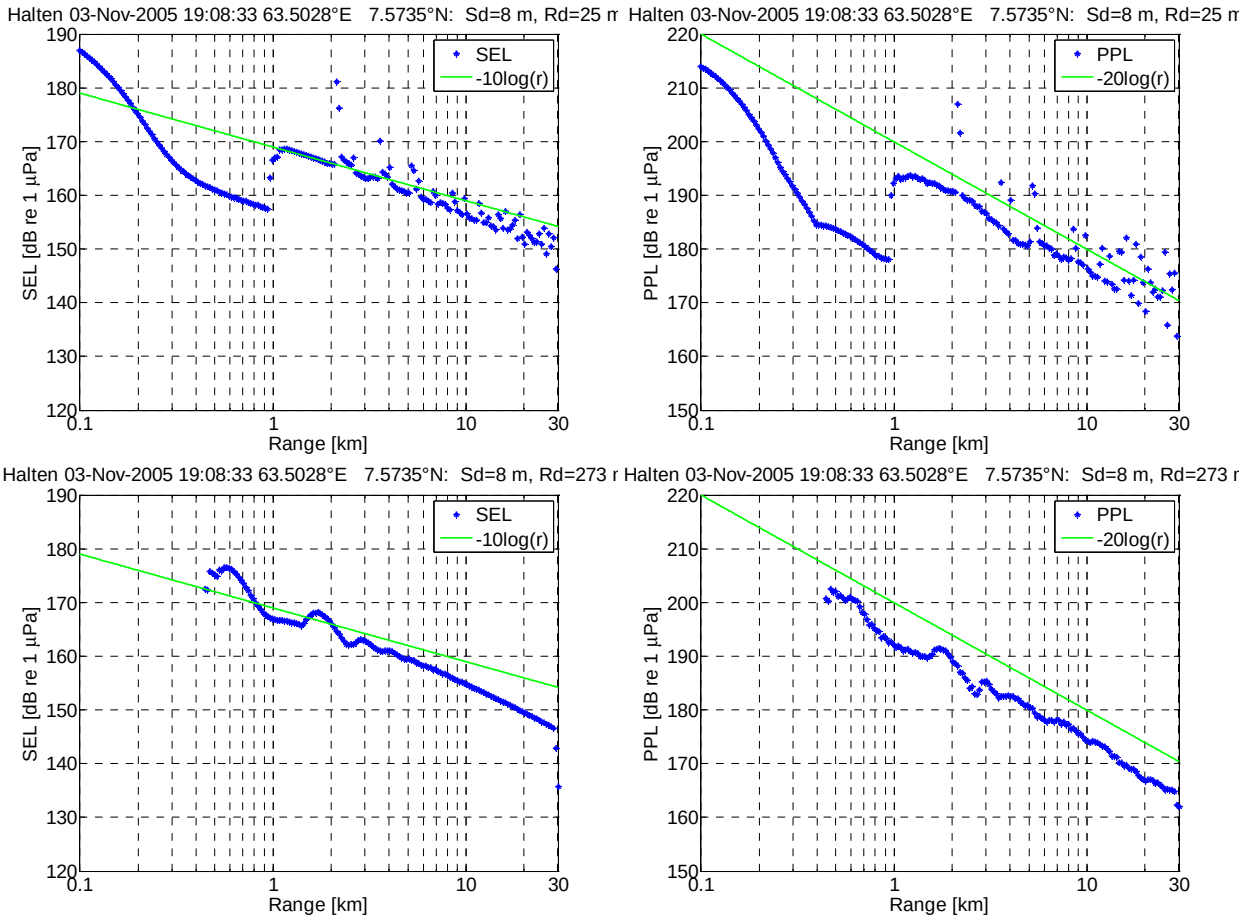

Figure 40 **Sound exposure level (SEL) and peak pressure level (PPL) for the Halten Bank autumn sound speed profile. Above: Receiver at 25 m depth, Below: Receiver at 273 m, 25 m above the bottom.**

6.5.1 Startle Threshold – Autumn

In Figure 41 the triggered startle response from the autumn sound speed profile can be seen. Due to the local hot-spots the shallow receiver exceeds the threshold limit further than the deep receiver. For the shallow and deep receiver the critical ranges are 21.3 km and 17.4 km, respectively.

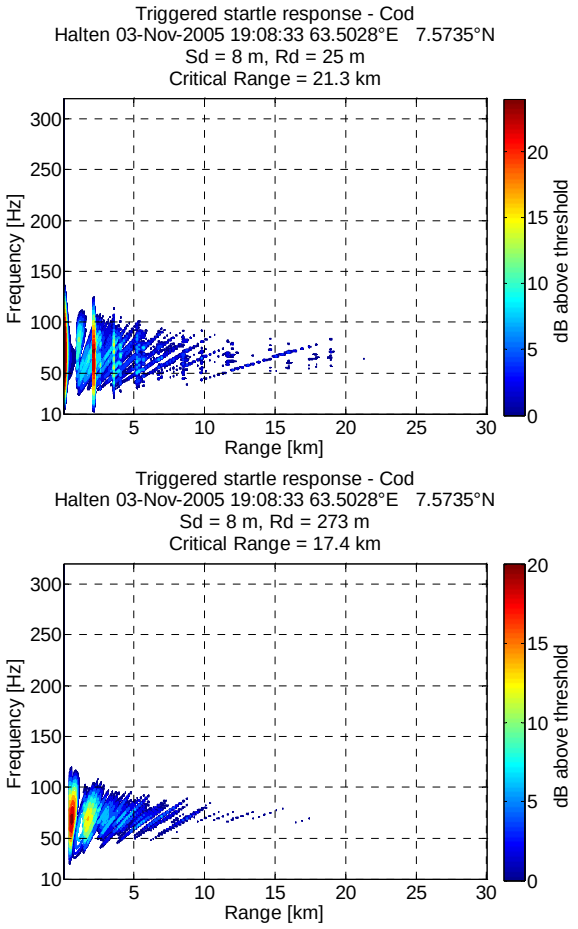

Figure 41 **Triggered startle response for the modeled result from the Halten Bank. The sound speed profile used is from November 2005. Above: Receiver at 25 m depth. Below: Receiver at 273 m, 25 m above the bottom.**

7 Discussion

Analyzing the recordings from the field Nordland VII showed that both the SEL and PPL had a clear decrease in level from approximately 3 km distance to approximately 18 km. The PlaneRay model has a similar decrease in the levels. Tests done with different bottom sediments and sound speed profiles showed that this decrease was mainly an effect of the increased depth at this range. The decrease was, however, affected by the sound speed profile to some extent.

Another finding was that the PPL followed the theory of spherical spreading, i.e. *-20 log(r)*, in the range with almost constant depth. The SEL followed close to cylindrical spreading, i.e. *-10 log(r)*, in the same range. In the already mentioned range from 3 – 18 km there was a decrease in level, breaking with the spherical and cylindrical spreading. This shows that the bathymetry has a large impact on the critical range, and that one should not blindly use the cylindrical and spherical spreading without consideration of the depth.

When a winter sound speed profile was used in the model in the Nordland VII scenario, the pronounced decrease in levels was reduced. This might be due to the fact that the sound speed profile bends the sound waves toward the surface, reducing the impact of the bathymetry.

Regarding the startle threshold for cod the limits were based on measurements done by the University of Oslo. In their measurements a probability of 0.1 was used. This means that only 1 out of 10 fish had to show a response for the measurement to be treated as above the threshold. In their setup this was the lowest probability possible, hence the thresholds used are the lowest values the University of Oslo could find.

Both the real measurement and the modeled impulse responses from the field Nordland VII were transferred to the frequency domain and compared to the threshold limits for cod. For the real measurements the results showed that they went below the threshold around 5 km, then it came back again around 20 km and stayed above throughout the 30 km limit. Since the threshold was exceeded with 1 – 2 dB only, it is assumed that the results would have gone below the threshold just above 30 km.

The modeled results showed that the source signal used was missing some frequency components. The main energy was, however, located around the same frequency, approximately 50 Hz. This is also the frequency region where the threshold limit is exceeded furthest in the real measurements, making it the most important when considering the critical range. The model showed good correlation with the real measurement up to the first limit at 5 km. It did not, as the real measurement, come back around 25 km. A closer look at the modeled results showed, however, that there was a reoccurring area around 20 – 30 km, but the values were just below (2 dB) the threshold limit. Since the real measurements were just above the threshold and the modeled results were just below, the total difference between them is not very large (< 5 dB). This does, however, show that small differences can have large effect on the critical range. One should therefore take a close look at the results before concluding with a critical range.

In the modeling of the Halten Bank different seasonal sound speed profiles where considered. The model used a flat seabed to only focus on the sound speed profiles and looked at receivers close to the surface and the bottom. These simulations showed large variations, both between seasons and between the two receivers. Sound speed profiles with positive gradient along the depth show that the surface receiver will have hot-spots (caustics) creating large peaks locally along the range. The location and intensity of these hot-spots are very sensitive to small variations in the oceanographic conditions, meaning one should not focus too much on the details around them. If the model gives such hot-spots, they will also exist in the real scenario, but it is very difficult to say where and how large they will be. Since the vessel with the airguns is moving, the hot-spots will, however, sooner or later hit most locations along the range.

The simulation of the Halten Bank with the summer profile showed that this profile gave the smallest difference between the surface and bottom receiver. The bottom receiver is also less affected by the seasonal variations than the surface receiver.

One source of error in the threshold responses is the sound exposure used in the fish tank for the threshold measurements. Since the fish tank is very small compared to the wavelength of interest, the sound field inside the tank will not be a plane wave. In the real situation with seismic shooting the sound will, at least when the distance is larger than the depth, be a plane wave. This could result in a different threshold for the fish, which in the tank will experience a more diffuse sound field than in reality. How the effect will be, if any, is impossible to say without more experiments.

When doing seismic surveys the source consists of several airguns in an array. This array is optimized to have maximum constructive interference in the vertical direction. Maximizing the constructive interference is done by shooting the different airguns at different time and with different amplitude. It is possible to implement this in PlaneRay, but since we did not have the exact time and amplitude for the array it was not taken into account. Such implementation would decrease, at least the peak levels, but maybe also the total amount of energy, from the source.

8 Conclusions

This project found good correlation between the real measurements, done at Vesterålen, and the modeled version of the same scenario when it came to sound exposure level and peak pressure level. Even if the critical range is very different between the two, the difference in level between the measured impulse responses and the modeled ones are not large. In the measured impulse responses the threshold is only exceeded by 1 – 2 dB in the range around 25 km, while the model is approximately 2 dB below the threshold at the same range.

The correlation between the measured and modeled results show that it should be possible to model the minimum distance the seismic airgun array should have to fish, not to trigger the startle response. This modeling can be done prior of seismic surveys to avoid any conflicts with commercial fishery.

Modeling the seasonal variation in the sound speed profiles also showed that a receiver close to the surface is more affected by this variation than the bottom receiver. The results also show that sound speed profiles with a positive gradient along the depth gives most variation at the surface receiver. A positive gradient bends the sound waves towards the surface, leading to local hot-spots, or caustics as it also is called.

The modeled shooting line, shooting line 1344, was located directly on the continental shelf. On the shelf the depth suddenly goes from approximately 100 m to more than 2 500 m. This is an atypical region of doing seismic surveys and a challenging bathymetry to model. A flat seabed, as the one used in the modeling of the Halten Bank, is more typical for seismic surveys and would be interesting to compare modeled results with real measurements.

For future seismic surveys we would also recommend to do an impact study before the shooting is began. If adequate data of the bathymetry, bottom sediments and source is fed into the PlaneRay model, important properties can be found and the noise impact to the environment can be reduced.

Bibliography

1. Hovem, J.M., *PlaneRay: An acoustic underwater propagation model based on ray tracing and plane wave reflection coefficients.* Theroretical and Computational Acoustics, 2007: p. 273-289.
2. NGU. *Classification of sediments based on grain size composition*. 2009 [cited 2010 June 15]; Available from: http://www.ngu.no/Mareano/Grainsize.html.
3. Hamilton, E.L., *Acoustic Properties of Sediments*, in *Acoustics and Ocean Bottom*, L. Lara-Sáenz, Prof., C. Ranz-Guerra, Dr., and C. Carbó-Fité, Dr., Editors. 1987, Consejo Superior de Invertigaciones Cientificas (C.S.I.C.): Madrid.
4. Løkkeborg, S., et al., *Effects of seismic surveys on fish distribution and catch rates of gillnets and longlines in Vesterålen in summer 2009*. 2010, The Institute of Marine Research.

SINTEF IKT
SINTEF ICT
Address:
Postboks 4760 Sluppen
NO-7465 Trondheim
NORWAY

Telephone:+47 73593000
Telefax: +47: 73592730

postmottak.IKT@sintef.no
www.sintef.no
Enterprise /VAT No:
NO 948 007 029 MVA

Project memo

Supplement 1 – Modeling of seismic noise

VERSION	**DATE**
0.1	2010-12-21

AUTHOR(S)
Jens M. Hovem

CLIENT(S)	**CLIENTS REF.**
The Norwegian Petroleum Directorate	Jan Stenløkk

PROJECT NO.	**NO. OF PAGES AND APPENDICES:**
90E322	10

ABSTRACT
This memo is a supplement to the SINTEF report A14560, January 2010-02-02, and deals with issues related to the use and the accuracy of the PlaneRay program for modeling seismic noise. The issues discussed are the use of plane wave reflection coefficients, the behavior of the model at caustics, and the reciprocity principle.

PROJECT MANAGER	SIGNATURE
Jens M. Hovem	

APPROVED BY (NAME, POSITION)	SIGNATURE
Odd Kr. Ø. Pettersen	

PROJECT MEMO NO.	**CLASSIFICATION**
Prosjektnotatnummer	Unrestricted

SINTEF

Document history

VERSION	DATE	VERSION DESCRIPTION
0.1	2010-12-21	Draft

SINTEF

Table of contents

SINTEF

Supplement 1 – Modeling of seismic noise

1 The use of plane wave reflection coefficients

A fundamental assumption of model is that the interactions with the boundaries are adequately described by plane wave reflection coefficient. In this section the validity of this assumption is investigated
Consider the situation depicted in 0 where the source and the receiver are located at heights z_r and z_s above an interface between two media 1 and 2 with sound speeds c_1 and c_2, and densities ρ_2 and ρ_1, respectively.

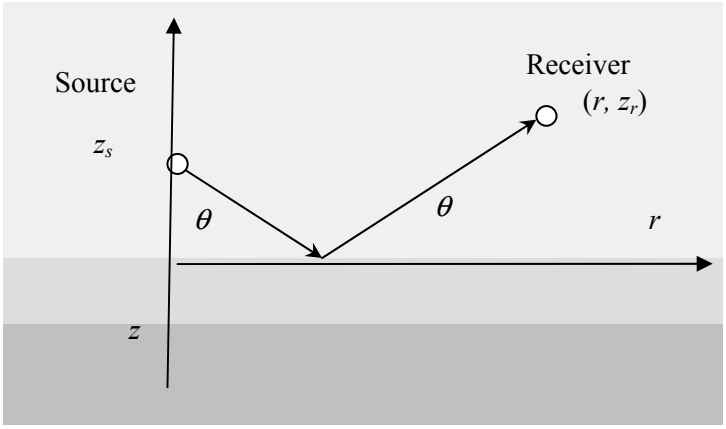

Figure 1 *The point source is at height z_s and the receiver is at height z_r above the interface between two media. The horizontal distance between the source and receiver is r. The arrows indicate the ray paths in the specular direction.*

The general expression for the reflected field is given in text books, as an integral for instance over horizontal wave numbers k, [Brekhovskikh, and Lysanov (2003)] as

$$\Phi_{ref}(r,z_r,\omega) = \frac{S(\omega)}{8\pi i}\int_0^\infty \Re(k)\frac{\exp\left(i\gamma_1|z_r+z_s|\right)}{\gamma_1} kH_0^{(1)}(kr)\,dk \quad . \tag{1}$$

$\Phi_{\text{ref}}(r, z_r\,\omega)$ is the reflected field due to point source with frequency ω and source strength $S(\omega)$, $\Re(k)$ is the reflection coefficient. $H_0^1(kr)$ is the Hankel function of first kind, which represents a wave progressing in the positive r-direction. The horizontal wave number k is related to the grazing angle θ by

$$k = \frac{\omega}{c_1}\cos\theta . \tag{2}$$

Equation (1) states that the field is given as an integral over all horizontal wave numbers, or as consequence of Equation (2), an integration over all real and the imaginary angles.
Consider now the situation where $\Re(k) = \Re$ is constant and independent of k or the angle. The integral in Equation (1) then becomes a standard integral and the exact result can be expressed as

$$\Phi_{ref}(r,z_r,\omega) = \frac{S(\omega)}{4\pi R_1}\Re\exp(ikR_1). \tag{3}$$

SINTEF

$$R_1 = \left[r^2 + \left(z_s + z_r \right)^2 \right]. \qquad (4)$$

According to Equations (3) and (4) the reflected wave is the same as the outgoing spherical wave from the image of the source in the mirror position of the real source and modified by the constant reflection coefficient $\Re$. The situation with a constant reflection coefficient is valid for perfectly flat sea surface where the reflection coefficient is equal to -1 for all angles of incidence. Thus the reflection from a smooth sea surface is accurately described plane wave reflection coefficients.

In the general case, and for reflections from the bottom, the reflection coefficient $\Re(k)$ is not constant and the integral can only be solved approximately or numerically. In order to derive an approximation the of the integral in Equation (1) the Hankel function is expressed in a power series with the first terms giving

$$H_0^1(kr) \approx \sqrt{\frac{2}{\pi kr}} \exp\left[i\left(kr - \pi/4 \right) \right] \left[1 + \frac{1}{8ikr} + \cdots \right] \qquad (5)$$

This is a valid approximation for fields at distances much longer than the wavelength. Restricting the integral of Equation (1) to the first term yields

$$\Phi_{ref}(r, z_r, \omega) = \frac{S(\omega)}{4\pi} \frac{1}{\sqrt{2\pi r}} \int_{-\infty}^{\infty} \Re(k) \frac{\sqrt{k}}{\gamma_1} \exp\left[ikr + i\gamma_1 \left(z_r + z_s \right) \right] dk \qquad (6)$$

Since the exponential in the integrand will normally be a rapid varying function the value of the integral is expected to be very small except for the values where the phase term of Equation (6) is nearly constant. The phase term of Equation (6)

$$\alpha = \left(i\gamma_1 \left| z_r + z_s \right| + ikr \right) \qquad (7)$$

The stationary points are defined to the values of the horizontal wave number *k* where the derivative of the phase with respect to *k* is equal to zero, that is where $d\alpha/dk$=0. In this

$$r = \frac{\left(z + z_s \right)}{\tan\left(\theta_0 \right)}. \qquad (8)$$

These locations of *r* correspond to the ray indicated in Figure 1. The result is quite simple, the reflected wave field is equal to that of the image source multiplied with the reflection coefficient at the specular angle.

There are however situations where this approximation is not sufficient in practice and this is discussed by Brekhovskikh and Lysanov (2003) and in the following we use their results without proof.

The plane wave reflection coefficient result is always valid for the perfectly reflection boundary. Thus it is correct to apply the plane wave reflection coefficient for the sea surface. For the reflection form the bottom the use of plane wave reflection coefficients represents an approximation. The accuracy of the approximation depends on the source or receiver distance from the bottom interface. The result of the analysis is that the distance *z* from the bottom must satisfy

SINTEF

$$z >> \frac{\lambda}{2\pi} \frac{\frac{\rho_b}{\rho_w}}{\sqrt{\left(\frac{c_b}{c_w}\right)^2 - 1}} \qquad (9)$$

With the water parameters of ρ_w = 1000 kg/m3 and c_w=1500 m/s, and the bottom parameters of ρ_b = 1500 kg/m^3 and c_b=1700 m/s. Equation (9) gives the requirement of z>> 0.5 λ. for the validity of using plane wave reflection coefficient at the bottom interface. At a much harder bottom with ρ_b = 1800 kg/m^3 and c_b=3000 m/s, we get that z>> 1.0 λ. Hence the condition for validity is somewhat easier to satisfy for a soft bottom than for a hard bottom.

2 Caustics and turning points

The acoustic intensity is calculated using the principle that the power within a space limited by a pair of rays with initial angular separation of $d\theta_0$ and centered on the initial angle θ_0, will remain between the two rays regardless of the rays' paths. The acoustic intensity as function of horizontal range $I(r)$ is, according to this principle, given by

$$I(r) = I_0 \frac{r_0^2}{r} \frac{\cos\theta_0}{\sin\theta} \left| \frac{d\theta_0}{dr} \right| \quad . \qquad (10)$$

In Equation (10), the initial angle at the source is denoted θ_0 and θ is the ray angle at the receiver position, which is at the horizontal range r from the source. The equation predicts infinite intensity under two conditions, when θ=0 and when $dr/d\theta_0$=0. The first condition signifies a turning point where the ray path becomes horizontal; the second condition occurs at points where an infinitesimal increase in the initial angle of the ray produces no change in the horizontal range traversed by the ray. The locations where $dr/d\theta_0$=0 are called caustics with infinite intensity as predicted by Equation(10). In reality there is focusing of energy to a very high level, but the actual level is not determined by classical ray theory. The problems with calculation the acoustic field at caustics and turning points represents a limitation with ray theory, which will be illustrated in the presented examples.
There exists theories to amend and repair the defects of ray theory at these points [Officer (1958), Brekhovskikh and Godin (2002), and Jensen et al. (1993)], but such theories are not implemented in the model. PlaneRay only detects the locations of the turning points and caustics, but accepts the amplitudes as resulting from the numerical evaluation of Equation (10)

Figure 2 shows details of the field at a caustic, with the upper plot showing the rays with initial angles in the range of – 6° to -1 and the lower part the geometrical transmission loss calculated numerically from Equation (10). Figure 3 shows the time response for 7 ranges in the interval from 1.6 km to 1.9 km. In this case, the source signal is a Ricker pulse with a peak frequency of 200Hz. Notice the effect of the 90° phase shift for ranges beyond the caustic at 1760 m and that the amplitude there is considerable higher.

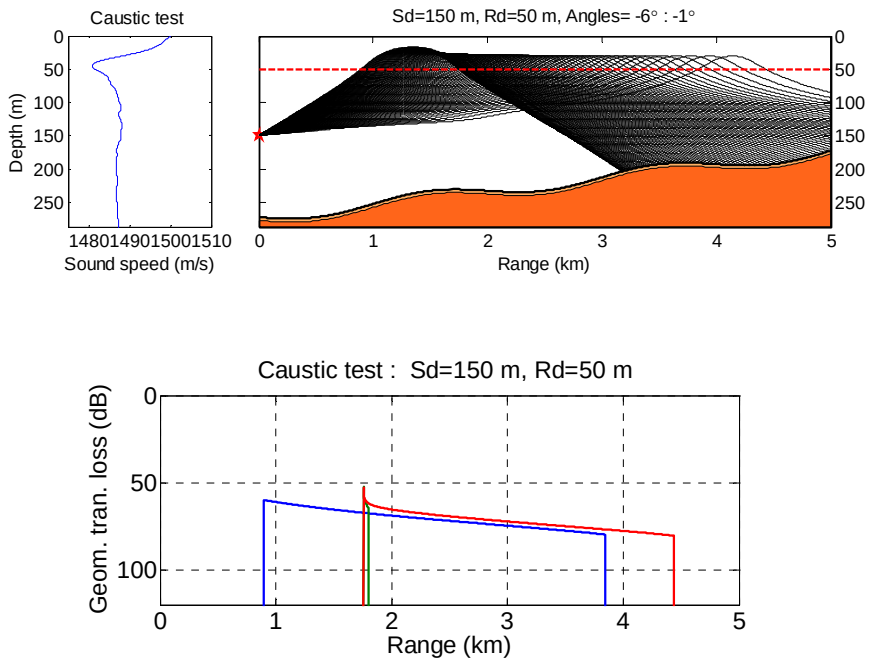

Figure 2 *Rays through a caustic (upper) and geometrical transmission loss as function of range (lower)*

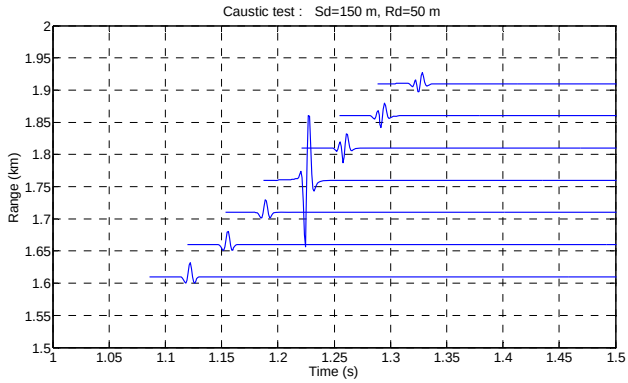

Figure 3 *Time responses around the caustic at 1.76 km. The transmitted signal is a Ricker pulse with peak frequency of 200 Hz.*

3 The principle of reciprocity and its validity for ray modeling

The principle of reciprocity is an important and useful property of linear acoustics and systems theory. Applied to the modeling of wave propagation the principle of reciprocity stipulates that the sound pressure at a position *B* due to a source at position *A* is equal to the pressure at *A* due to a similar source at *B*. The principle is very general and valid also in cases where the wave undergoes reflections and refraction at boundaries on its path from source to receiver. [Landow L. D., and F. M. Lifshitz (1959)].

Figure 4 (a) shows a situation where we want to calculate the received field receiver at a fixed observation position *B* generated by a moving source at position *A*. Since the PlaneRay model assumes that the source is stationary and the receiver is moving, it may be more convenient to model the reciprocal situation as shown in Figure 4(b) where the bathymetry is flipped and the source and receiver depths are interchanged.

We test the reciprocity principle in practice and check its validity in the PlaneRay model. We chose the same scenario as before but the moving source is now a depth of 25 m and is emitting a short Ricker pulse

with main frequency 50 Hz. The fixed receiver is at 125 m depth in the actual situation [Figure 4(a)], in the reciprocal situation [Figure 4 (b)] the source and receiver depths are interchanged. The eigenrays for the two reciprocal situations are shown in Figure 5 where the two ray diagrams show the most significant eigenrays. Note that the two results are based on rays with a spread of +- 30° and +-45° respectively

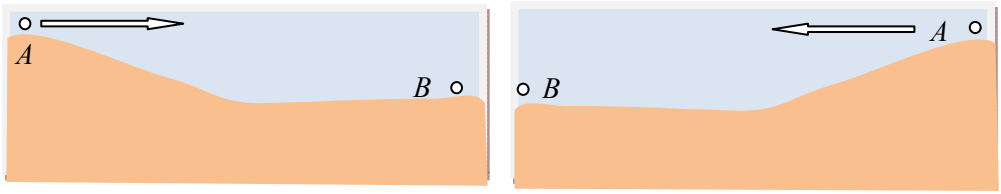

(a) (b)

Figure 4 *(a) The real situation with a moving source (A) and a stationary observer (B) (b) The reciprocal situation with a stationary source (B) and a moving receiver (A).*

In this example the bottom is modeled with a 10 m thick sediment layer over a homogenous solid half space. The sedimentary layer has a sound speed of 1700 m/c, attenuation 1 dB per wavelength and density of 1500 kg/m^3. The solid half space has a compressional sound speed of 2000 m/s, a shear speed of 200 m/s and density is 2000 kg/m^3. Both wave types have absorption of 1 dB/wavelength. Figure 6 presents the modeled time response for the two situations. The two results are nearly identical which proves as expected that the reciprocity principle is correctly represented in ray modeling.

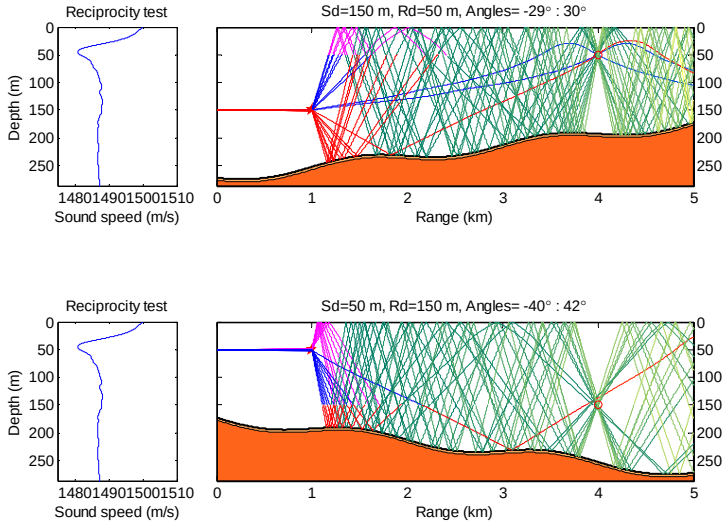

Figure 5 *Transmission over an undulating sloping bottom with a northern summer sound speed profile with the eigenrays for the two reciprocal situations.*

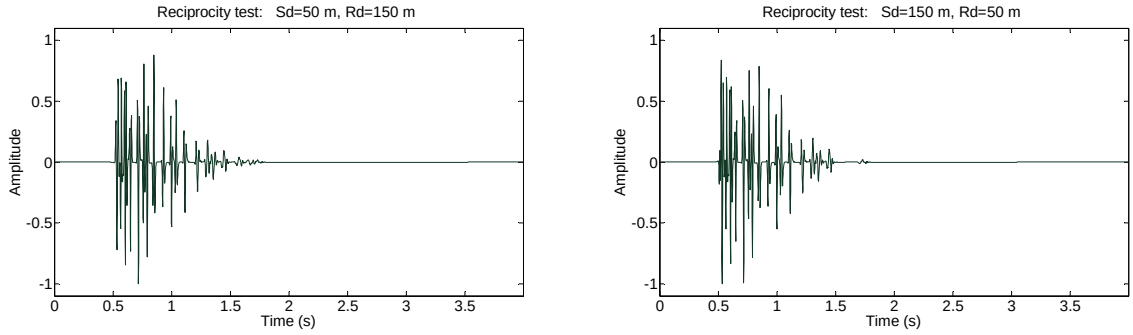

Figure 6 *Time signal from a source at position A (50 m) to receiver at position B (150 m) compared with the reciprocal situation with transmission from B to A.*

The reciprocity principle may be used for checking the validity of the modeling result. It is a good indication that the model result is correct if modeling the real case and the reciprocal situation yields the same result. In the example considered here the bathymetry is only slowly varying over the actual range and the PlaneRay result is correct. However, it is not difficult to envision much more rapidly changing bathymetry where PlaneRay may fail. Therefore, it is recommended to check the validity of the modeling results by comparing with modeling of the reciprocal situation.

Finally, it should be noted that the reciprocity principle only apply to point-to-point situations. This is illustrated in Figure 7 where transmission loss is plotted as function of source and receiver separation. The two figures are different, as they should be, since the bathymetries are not the same. The two transmission losses are only identical at 4 km separation where the two situations are identical as shown in Figure 7.

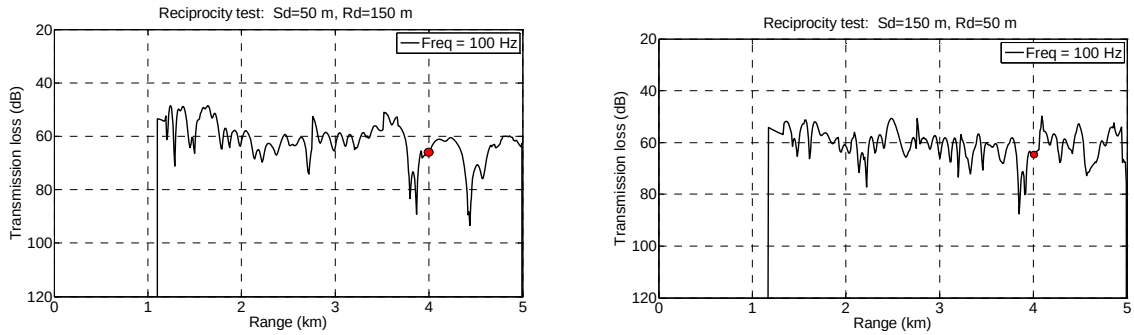

(a) (b)

Figure 7 *Transmission loss as function of distance for a source at position A to receiver at position B, compared with the reciprocal situation with transmission from B to A. The transmission loss at a separation of 4 km are identical is indicated with circles.*

References

Brekhovskikh, L. M., and O. A. Godin. *Acoustics of layered media I. Plane wave and quasi plane waves.* Springer-Verlag, Berlin, 2002.

Brekhovskikh, L. M., and Yu. P. Lysanov. *Fundamentals of ocean acoustics,* 3rd ed. Springer-Verlag, New York City, 2003.

Jensen, F. B., W. A. Kuperman, M. B. Porter, and H. Schmidt. *Computational ocean acoustics*. AIP Press, American Institute of Physics, Woodbury, New York City, 1994.

Landow, L. D., and E. M. Lifshitz. *Fluid Mechanics*. Pergamon Press, Oxford UK 1959.

Officer, C. B. *Introduction to the theory of sound transmission*. McGraw-Hill, New York City, 1958.

SINTEF IKT
SINTEF ICT
Address:
Postboks 4760 Sluppen
NO-7465 Trondheim
NORWAY

Telephone:+47 73593000
Telefax: +47: 73592730

postmottak.IKT@sintef.no
www.sintef.no
Enterprise /VAT No:
NO 948 007 029 MVA

Project memo

Supplement 2 – Source function and airgun array model

VERSION
0.1

DATE
2010-12-21

AUTHOR(S)
Jens Martin Hovem

CLIENT(S)
The Norwegian Petroleum Directorate (NPD)

CLIENTS REF.
Jan Stenløkk

PROJECT NO.
90E322

NO. OF PAGES AND APPENDICES:
15

ABSTRACT
In marine seismic surveys a number of air guns configured in a two-dimensional array are usually used. The purpose of this arrangement to achieve that the individual air guns interact to generate a sharp single pulse that propagates with the maximum energy in the vertical direction. Since the group of air guns cover an area relatively large compared with the acoustic wavelength, the directivity of the air gun group becomes important.
For the modeling of the seismic noise of the array we need to know the directional properties of the array i.e., the amplitudes and time structure of the transmitted signal in all directions, not only the vertical direction Such information is not readily available and therefore we have constructed a model for the directional properties of two-dimensional air gun arrays. This is a model for the directional properties of the source layout only and not a model of the physics of sound generation of air guns. This note describes the air gun array model and shows some effects.

The note in a supplement to the SINTEF report A14560, January 2010-02-02.

PROJECT MANAGER
Jens M. Hovem

SIGNATURE

APPROVED BY (NAME, POSITION)
Odd Kr. Pettersen

SIGNATURE

PROJECT MEMO NO.2
Prosjektnotatnummer

CLASSIFICATION
Unrestricted

SINTEF

Document history

VERSION	DATE	VERSION DESCRIPTION
0.1	2010-12-21	Draft

SINTEF

Table of contents

Contents

SINTEF

Source Function and Airgun Array Model

1 Introduction

In marine seismic surveys a number of air guns configured in a two-dimensional array are usually used. Figure 1 shows an example of layout with several clusters of single guns in groups with various spacing in the towing direction and in the cross direction. This particular configuration was used by PGS in a collaborative investigation with Institute of Marine Research (IMR) in the "Seismikk-tobis" project in 2002) [Hassel *et al*., ([2003; 2004)] The array consist of 28 active air guns in a rectangular grid of 20 time 15 meter. The volumes of the individual air guns ranged from 0.3 to 4 liter. The purpose of this arrangement to achieve that the individual air guns interact to generate a sharp single pulse that propagates with the maximum energy in the vertical direction. An example of such a pulse and its frequency spectrum is shown in Figure 2. Note that the peak pressure is about 60 bar, which is equivalent to 255 dB relative 1 μPa- a number we will use later in this report.

Since the group of air guns cover an area relatively large compared with the acoustic wavelength, the directivity of the air gun group becomes important.
For the modeling of the seismic noise of the array we need to know the directional properties of the array i.e., the amplitudes and time structure of the transmitted signal in all directions, not only the vertical direction as the signal shown in Figure 2. Such information is not readily available and therefore we have constructed a model for the directional properties of two-dimensional air gun arrays. This is a model for the directional properties of the source layout only and not a model of the physics of sound generation of air guns. This note describes the air gun array model and shows some effects.

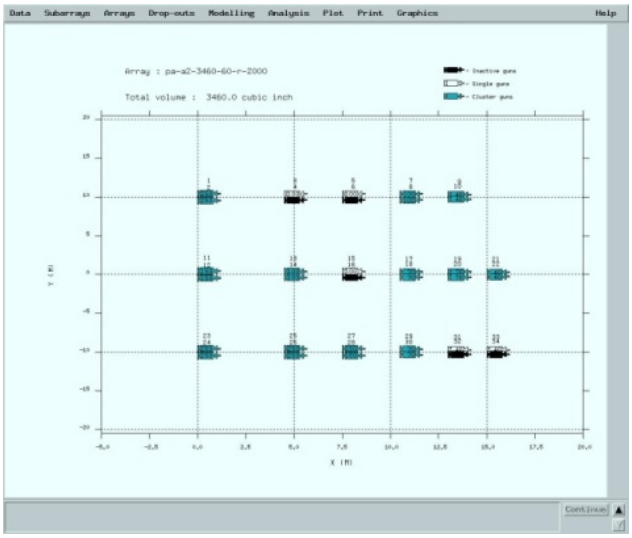

Figure 1 **Air gun layout used in field surveys (© PGS Geophysical). Green filled symbol represents two guns, open green symbol is a single gun and black symbols are inactive guns.**

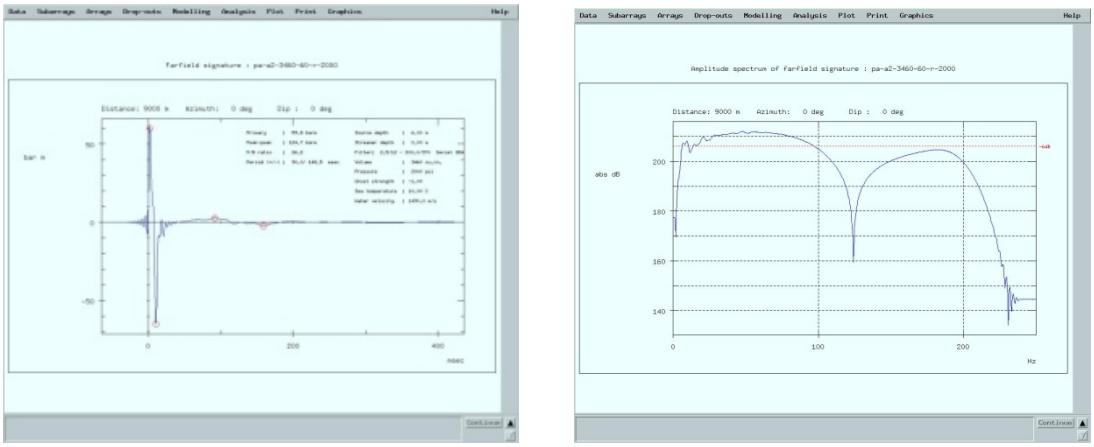

Figure 2 **Time response and, frequency spectrum of the air gun array without surface ghost in the vertical direction under the array. The pulse amplitude of refers to a reduced distance of 1 meter (© PGS Geophysical).**

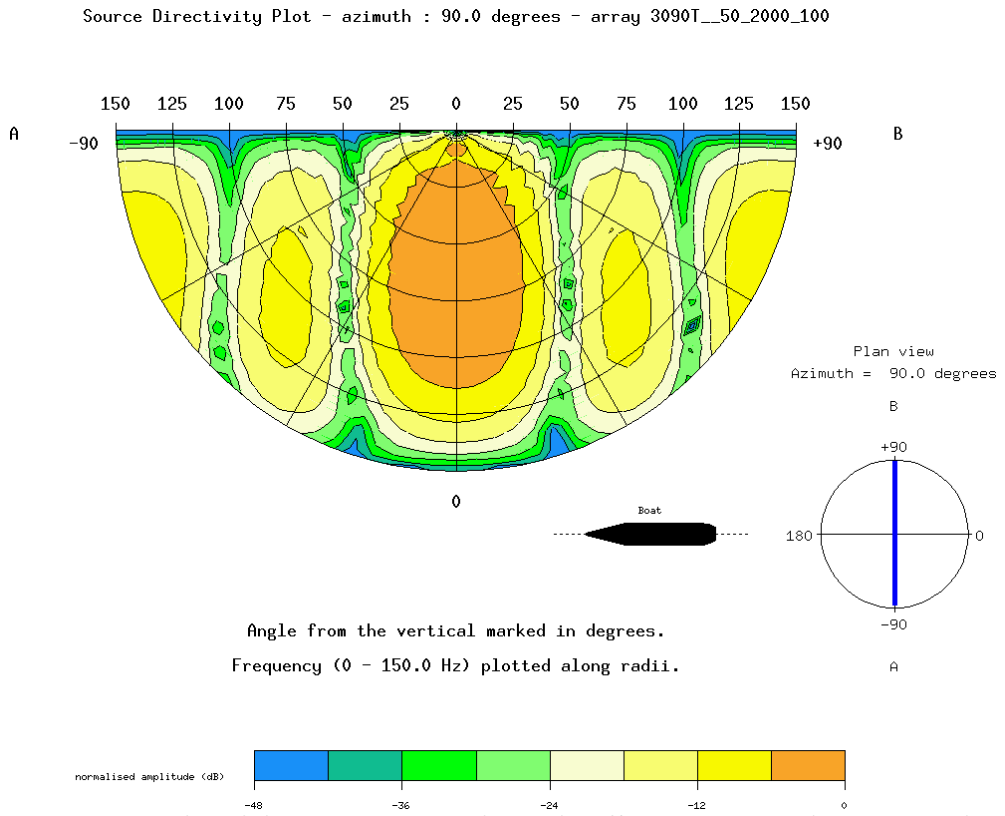

Figure 3 **Modeled directivity at an observation point 60 m below the airgun array in Figure 2. Along ship above and athwart ship below. (© PGS Geophysical).**

SINTEF

2 Modeling

The modeling implemented in PlaneRay may be considered in two parts; (1) the modeling of a single source function, and (2) the modeling of the directional distribution of the array. The model derives both a time function $s(t)$ and the frequency function $S(\omega)$ of a single source, and an array model $A(\omega, \theta, \varphi)$, as a function of frequency and the spatial angles in elevation and azimuth. According to linear system theory, the spectrum, in frequency and directions, of a transmitted signal from the array is then

$$H(\omega,\theta,\varphi) = S(\omega)\,A(\omega,\theta,\varphi). \tag{1}$$

2.1 Modeling the single source function

In the PlaneRay model, the elements of the group are point sources transmitting short Ricker pulses. Figure 4 shows an example of a Ricker pulse, it this case with its main frequency components centered at 50 Hz, which is quite close to the actual signals used in the survey.

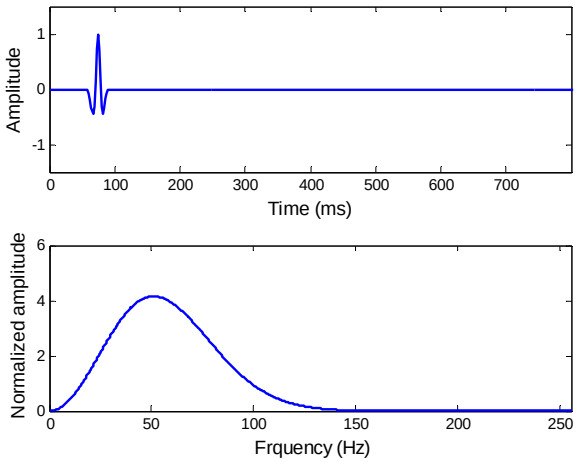

Figure 4 Ricker time pulse and frequency function.

2.2 Modeling the array directivity.

Figure 5 shows a typical air gun layout with N_x guns in the towing direction and N_y guns in the cross direction. Figure 6 shows the geometry of the problem. The array is in the x-y plane where z=0. The coordinate of a source point is (x_n, y_n) and the rectangular coordinates of the field point is x, y, z). The rectangular coordinates are related to the spherical coordinates by

$$\begin{aligned} x &= r\cos\theta\cos\varphi, \\ y &= r\cos\theta\sin\varphi, \\ z &= r\sin\theta. \end{aligned} \tag{2}$$

The distance between a source point in the x-y plane and the field point given by the spherical coordinates, r, θ and φ are, from Figure 6, given by

$$R = \sqrt{(r\cos\theta\cos\varphi - x_n)^2 + (r\cos\theta\sin\varphi - y_n)^2 + (r\sin\theta)^2} \tag{3}$$

The farfield approximation of this expression is

SINTEF

$$R \approx \sqrt{r^2 - 2rx_n \cos\theta\cos\varphi - 2ry_n \cos\theta\sin\varphi}$$
$$\approx r - x_n \cos\theta\cos\varphi - y_n \cos\theta\sin\varphi \qquad (4)$$

With a number of sources at position (x_n,y_n) and with source strengths and spectrum $S_{n,m}(\omega)$ the directivity function for a particular frequency f is expressed by the sum

$$A(\omega,\theta,\varphi) = \sum_{n,m} S_{n,m}(\omega) \exp\left[-2\pi i \frac{(x_n \cos\theta\cos\varphi - y_n \cos\theta\sin\varphi)}{\lambda}\right]. \qquad (5)$$

The acoustical wavelength is $\lambda=c/f$, c is the sound speed and f is the frequency. Equation (5) is the general expression valid for any number of sources with different frequency spectrum and locations. For simplicity, we assume that all sources emit identical signals with the same spectrum. With adequate information of the source positions x_n and y_n and the source strength $S_{n,m}$

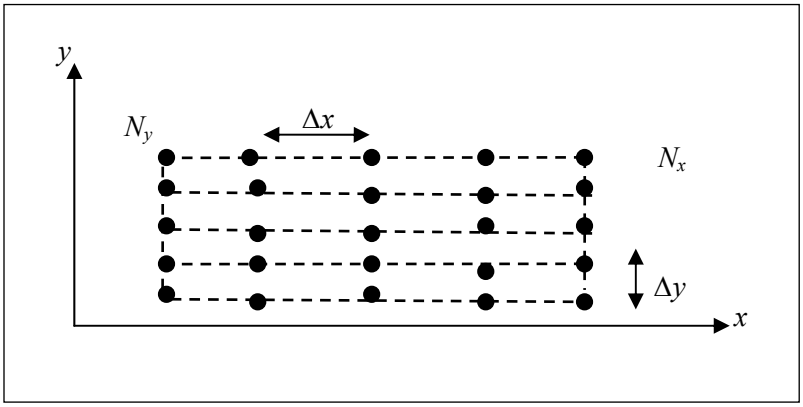

Figure 5 **Air gun layout with regular spacing with N_x guns at equal spacing Δx in the x direction and N_y guns in the y direction with spacing Δy.**

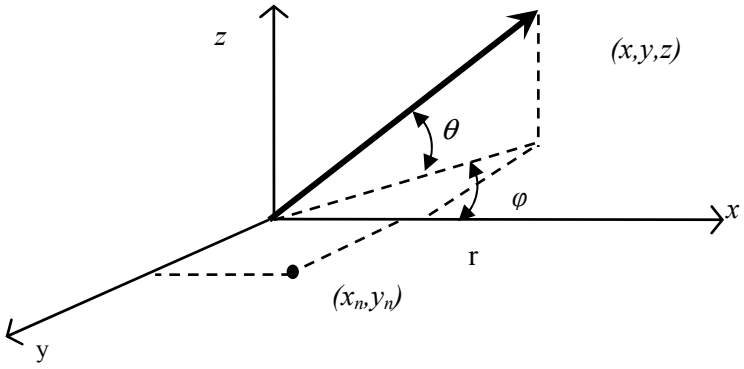

Figure 6 **Geometry of the model situation. A source point is in the position x_n, y_n and the field point is at x, y, z and given by the distance r and the angles φ and θ.**

Considering the special case when the sources are of equal strengths and spaced on a rectangular grid with spacing Δx and Δy and with N_x and N_y sources in the x direction and y direction, respectively, i.e.,

SINTEF

$$x_n = n\Delta x,\ n = 0,..N_x - 1,$$
$$y_n = n\Delta y,\ n = 0,..N_y - 1. \tag{6}$$

Equation (5) produces

$$A(\omega,\theta,\varphi) = \left(N_x N_{xy}\right)\exp\left(-\phi\right)\left(\frac{\sin\left[\pi\frac{N_x\Delta x}{\lambda}\left(\cos\theta\cos\varphi\right)\right]}{N_x\sin\left[\pi\frac{\Delta x}{\lambda}\left(\cos\theta\cos\varphi\right)\right]}\frac{\sin\left[\pi\frac{N_y\Delta y}{\lambda}\left(\cos\theta\sin\varphi\right)\right]}{N_y\sin\left[\pi\frac{\Delta y}{\lambda}\left(\cos\theta\sin\varphi\right)\right]}\right), \tag{7}$$

where the phase factor is

$$\phi = \exp\left[-\pi i\left(\frac{N_x\Delta x}{\lambda}\cos\theta\cos\varphi\right)\right]\exp\left[-\pi i\left(\frac{N_y\Delta y}{\lambda}\cos\theta\sin\varphi\right)\right] \quad . \tag{8}$$

This phase factor represents a small time shift of no importance and is therefore ignored. The directivity function is defined by

$$B(\omega,\theta,\varphi) = \left(N_x N_y\right)\frac{\sin\left[\pi\frac{N_x\Delta x}{\lambda}\left(\cos\theta\cos\varphi\right)\right]}{N_x\sin\left[\pi\frac{\Delta x}{\lambda}\left(\cos\theta\cos\varphi\right)\right]}\frac{\sin\left[\pi\frac{N_y\Delta y}{\lambda}\left(\cos\theta\sin\varphi\right)\right]}{N_y\sin\left[\pi\frac{\Delta y}{\lambda}\left(\cos\theta\sin\varphi\right)\right]}. \tag{9}$$

The maximum occurs for the vertical directions where $\theta=\pm\pi/2$ corresponding to the straight down and up directions, and the maximum value is,

$$\max\left\{B(\omega,\theta)\right\} = \left(N_x N_y\right). \tag{10}$$

For the condition that $\varphi=0$, Equation (9) gives

$$B(\theta,0) = \left(N_x N_y\right)\frac{\sin\left[\pi\frac{N_x\Delta x}{\lambda}\left(\cos\theta\right)\right]}{N_x\sin\left[\pi\frac{\Delta x}{\lambda}\left(\cos\theta\right)\right]}. \tag{11}$$

This is the in-line directivity as function of elevation angle. Note that in this farfield approximation the directivity is not dependent on the athwart or y-distribution of sources and the directivity is as for a line array in the x-direction.

The azimuth directivity is obtained by setting $\theta=0$ Equation (7) gives

$$A(\omega,\theta,\varphi) = \left(N_y N_y\right)\exp\left(-\phi\right)\left(\frac{\sin\left[\pi\frac{N_x\Delta x}{\lambda}\left(\cos\varphi\right)\right]}{N_x\sin\left[\pi\frac{\Delta x}{\lambda}\left(\cos\varphi\right)\right]}\frac{\sin\left[\pi\frac{N_y\Delta y}{\lambda}\left(\sin\varphi\right)\right]}{N_y\sin\left[\pi\frac{\Delta y}{\lambda}\left(\sin\varphi\right)\right]}\right). \tag{12}$$

Figure 7 shows the directivities as function of θ calculated for φ=0 [Equation (11)].
Figure 8 shows the directivities as function of φ calculated for θ=0 [Equation (12)]. In both figures the frequencies are 50 Hz and 150 Hz.

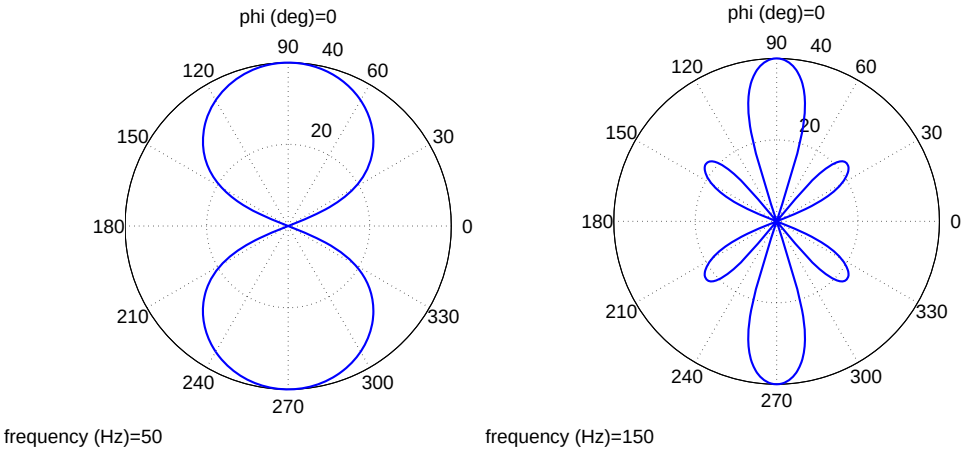

Figure 7 **Directivity pattern as function of the elevation angle θ for φ =0 for the frequencies of 50 and 150 Hz. N_x=20, Δx=5 m, N_y=5, Δy=10 m.**

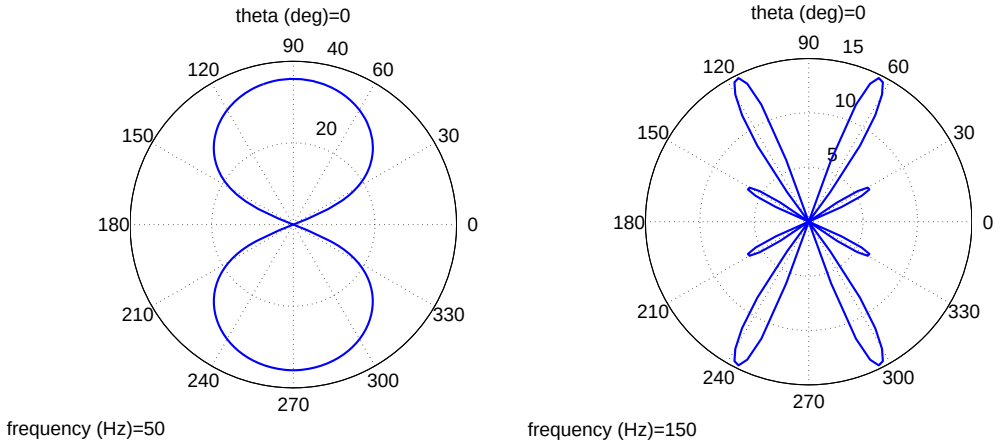

Figure 8 **Directivity pattern as function of azimuth angle φ for θ=0 for the frequencies of 50 and 150 Hz. N_x=20, Δx=5 m, N_y=5, Δy=10 m.**

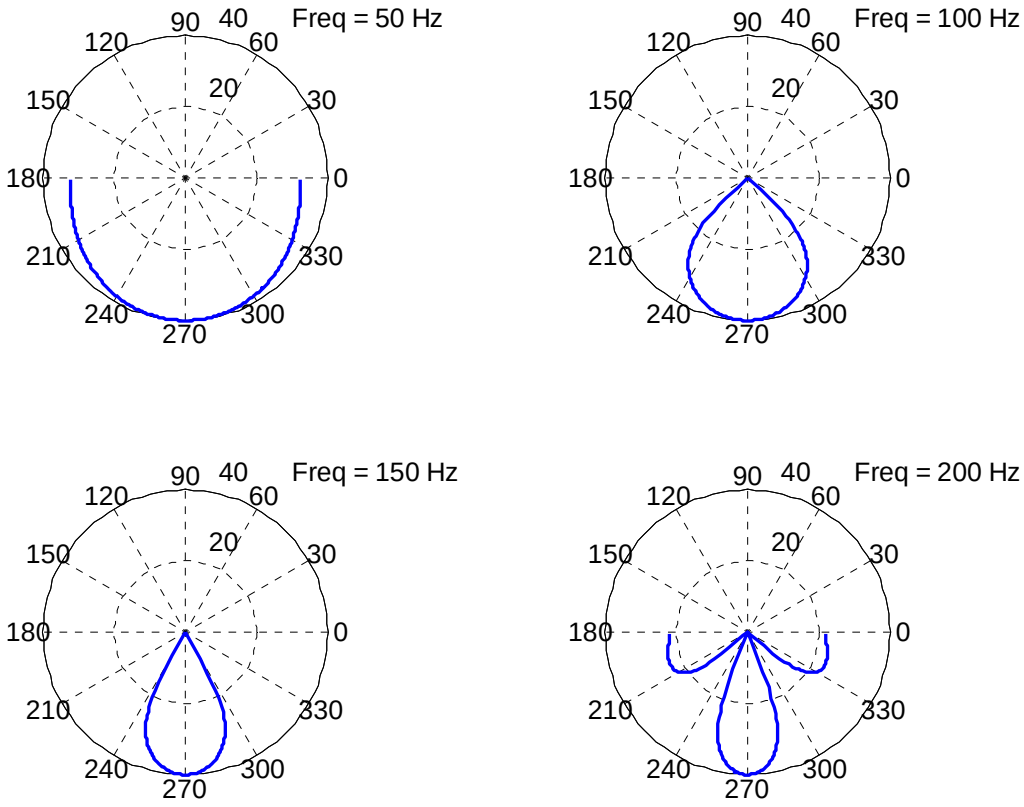

Figure 9 **Directivity pattern as function of elevation angle θ for the frequencies of 50, 100 150 1nd 200 Hz. N_x=8, Δx=2.5 m, N_y=1, Δy=0 m.**

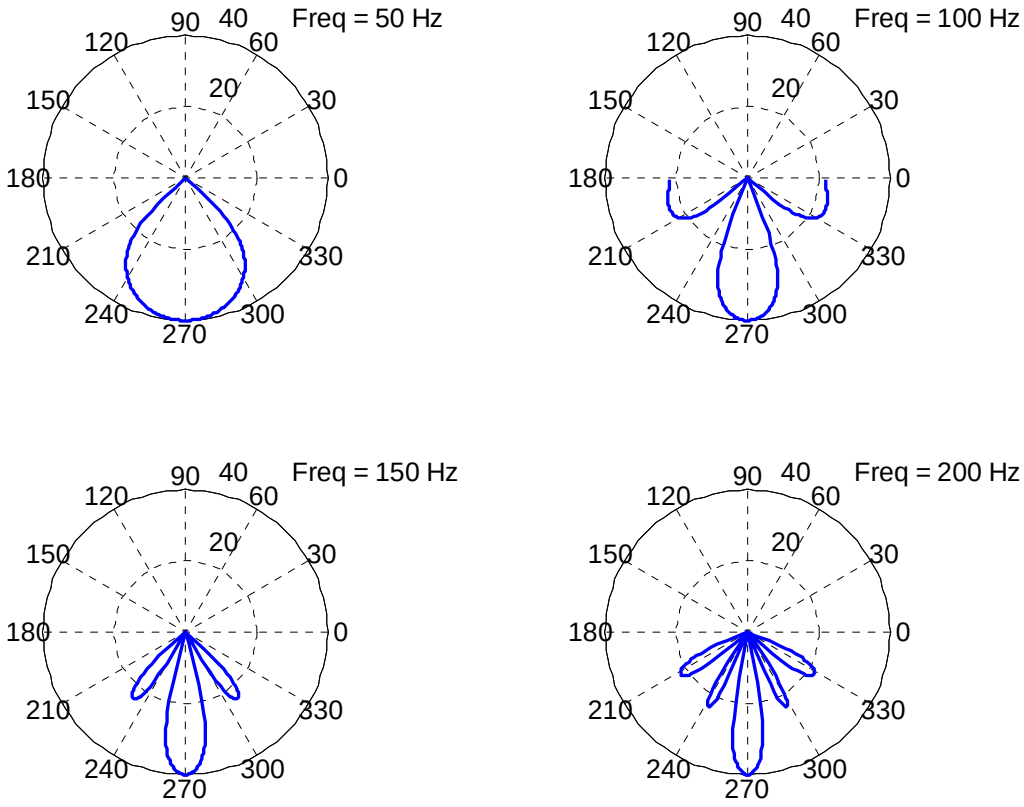

Figure 10 **Directivity pattern as function of elevation angle θ for the frequencies of 50, 100 150 1nd 200 Hz. N_x=8, Δx=5 m, N_y=1, Δy=0 m.**

SINTEF

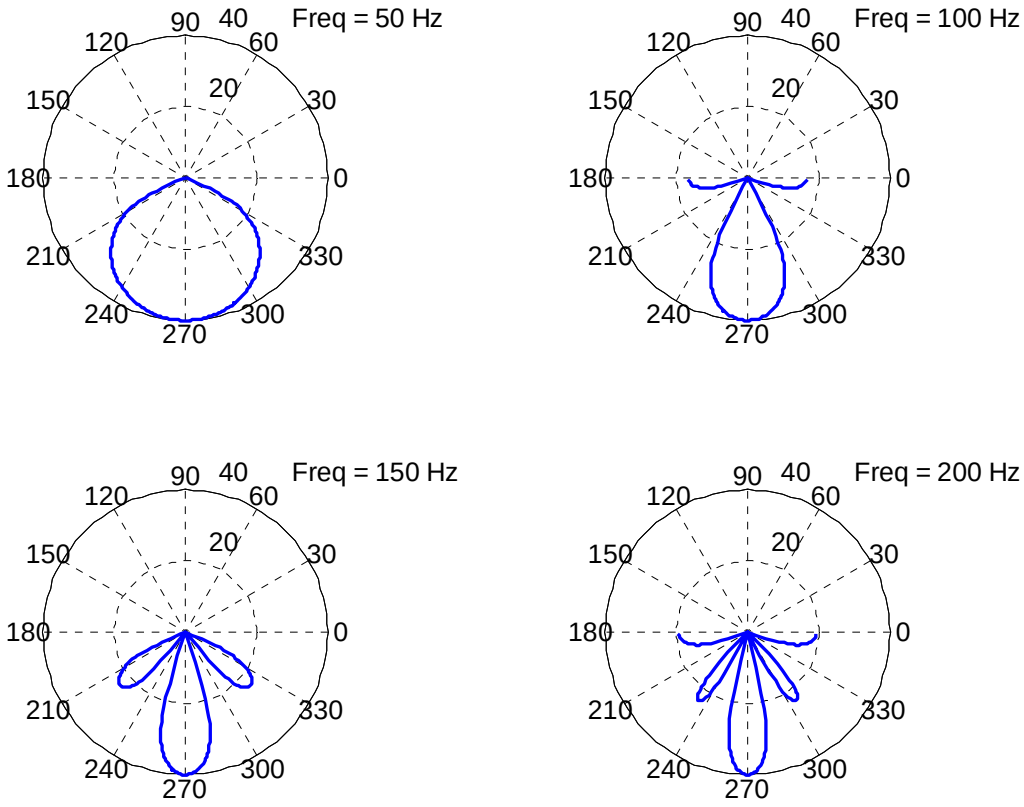

Figure 11 **Directivity pattern as function of elevation angle θ for the frequencies of 50, 100 150 1nd 200 Hz. N_x=8, Δx=4 m, N_y=1, Δy=0 m.**

These figures demonstrate that the directivity of an air gun group is a complicated function of frequency. Since we are dealing with transient and broad band frequency signal the frequency-domain description with a few frequencies is not very useful. Our approach is therefore to calculate the frequency- angle spectrum of Equation (9) for all the frequencies of the source function and transfer the result to the time domain by the use of a Fourier transform.

2.4 The combined model.

The frequency spectrum of a source with angles θ and φ is given by Equation (1). Figure 12 shows results of simulations of the time responses as function of elevation angle θ for the case that the azimuth angle φ=0 using Equation (11). In both plots in the figure the number of elements are N_x=8 and the inter element spacing is 100 m in the upper plot and 10 m in the lower plot. The 100 m spacing is unrealistic and shown only to illustrate the general directional properties, but the 10 m spacing in the lower plot is quite realistic. From the upper plot we see that the array of air guns generates a sequence o f N_x pulses separated in time with $\Delta t=(\Delta x/c)\cos\theta$. In the vertical direction of $\theta=\pi/2$ all the pulses add together and produces a single pulse with height that is a factor N_x higher than the individual pulses. The same thing is evident in the lower plot with the inter element spacing of 10 m, but now the time separation of the individual pulses are much shorter and the pulses are not separated in time.

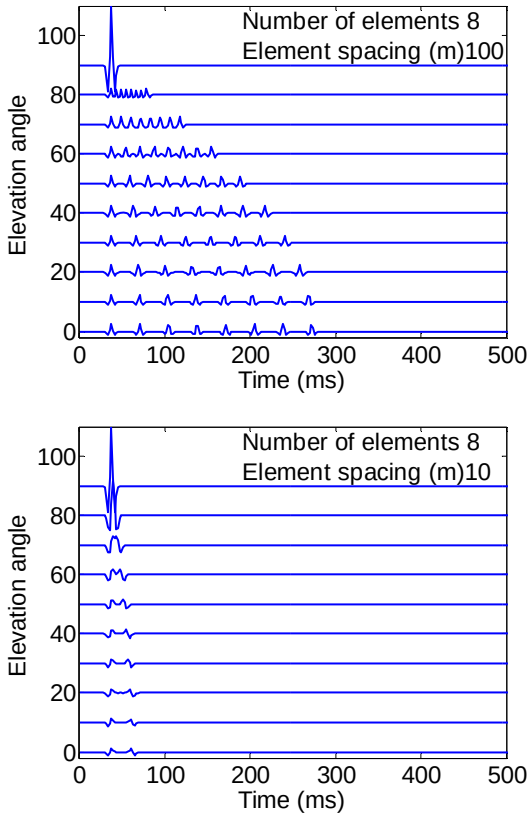

Figure 12 **Pulse shapes from a linear array as function elevation angle θ. The upper case has 8 elements spaced 100 m apart and the lower case has 8 elements spaced 10 m apart.**

Figure 13 shows results calculated by PlaneRay and intended to show the effect of the array directivity. The array has 8 elements spaced 10 m apart and each air gun produces a Ricker pulse with a time signature and frequency spectrum as shown in Figure 4.The receivers are located 100 m directly below the array and at horizontal distances from10 m to 100 m from the center of the array. The effect of amplitude reduction caused by spherical spreading has been removed and the figure therefore shows only the effect of the directionality of the air gun array.

The figure shows that the received at 10 m distance is almost a pure Ricker pulse, whereas the received signals at longer distances are spread out in time and consequently has considerable lower peak amplitude. This is in agreement with observations in of Figure 12 since the receiver at 10 m correspond to an angle θ equal to atan(100/10) which is 86 °and the receiver at 100 m is at an angle of 45°.

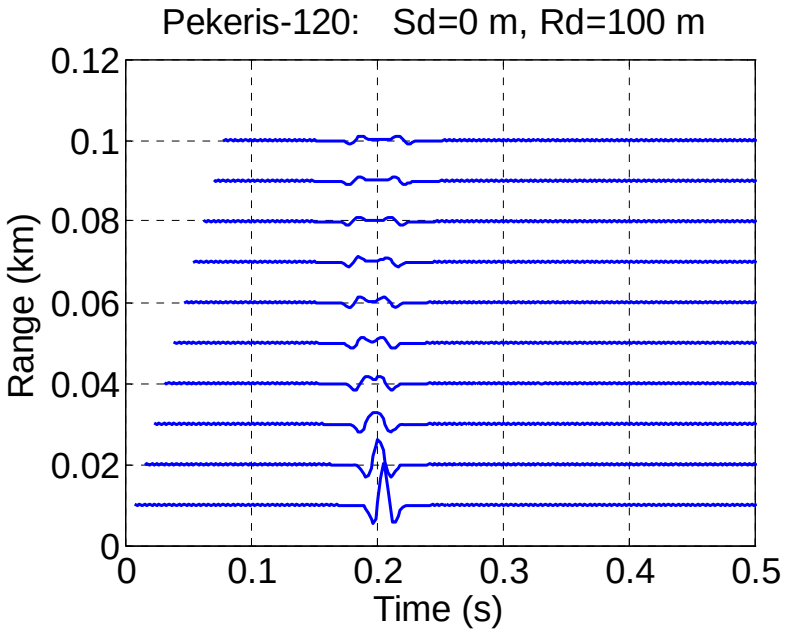

Figure 13 **The direct signal from an air gun array with 8 elements at 10 m spacing. The receiver at 100 m below the array and at horizontal distance from 10 m to 100 m. The effect of amplitude reduction caused by spherical spreading has been removed.**

3 A test case

A simple test is considered where the sound speed is constant equal to 1500 m/s and the water depth is 300m. The source depth is 8 meter and we consider two case (a) with a single source with peak pressure level of SL=255 dB and (b) an horizontal array with Ne=8 sources of equal strength equal to SL-20log(8) =237dB. When all sources are coherently added as the will in the straight downward the peak pressure kevel is 255 dB. All dB values relative to 1 µPa.

Figure 14 shows the time response for the two cases; notice the double pulse structure for the array responses. Figure 14 shows only the structure of the received multipath structure and not amplitude information since the plots are normalized with respect to the strongest peak in each plot.

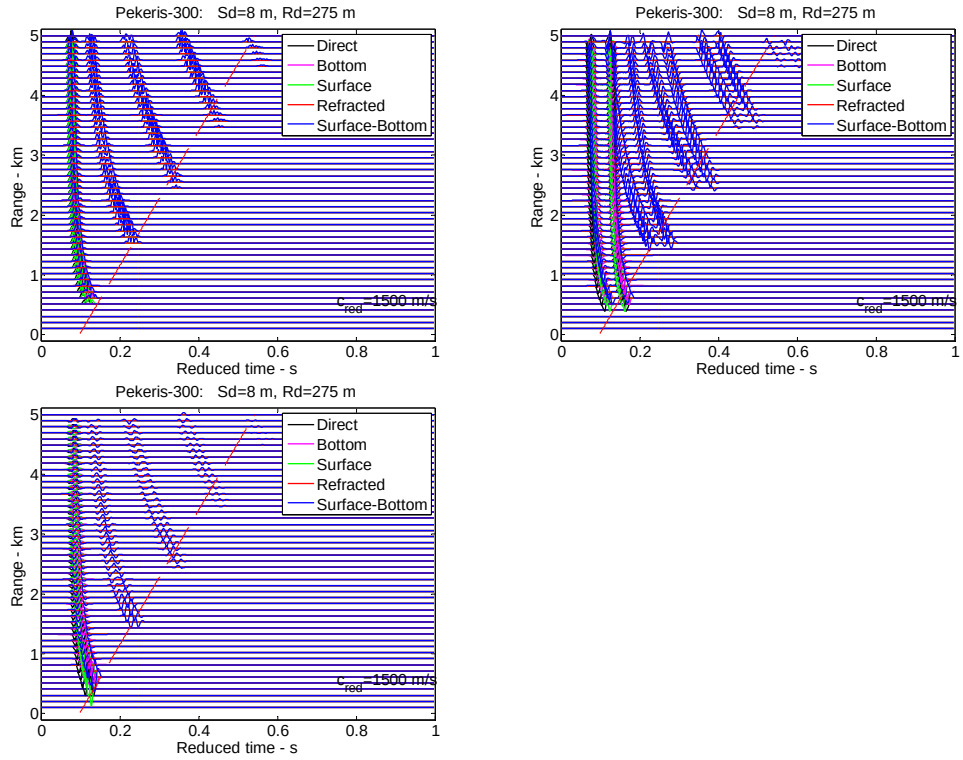

Figure 14 **Time response of received signals as function of range from 0.1 to 5 km. Left: A single source, Right: An array with 8 sources with 10 m spacing, below 2.5 m spacing**

Amplitude information is contained in the plots in Figure 15, Figure 16 and Figure 17, which shows peak pressure and rms. Pressure, respectively, as function of distance from the source.
The reduction in peak pressure is, as expected, 20log(Ne)= 18 dB .The rms pressure also seems to be reduced with the same number of dB, but in general this fluctuate significantly because of interference. A reduction of 10 log(Ne)=9 dB may be more typical.

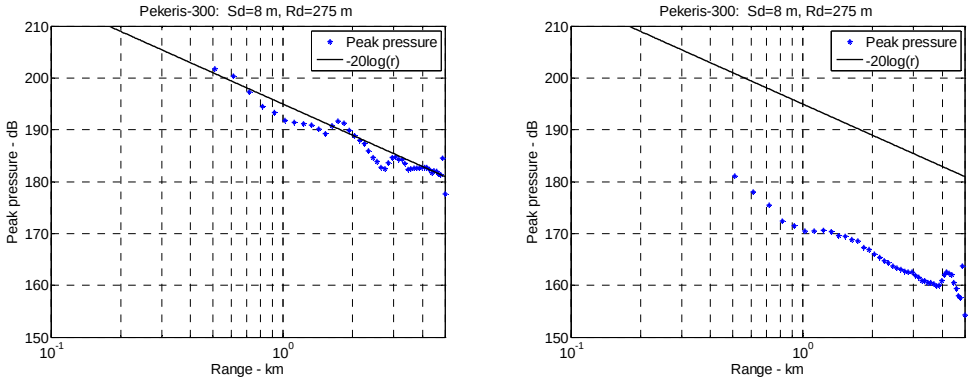

Figure 15 **Peak pressure as function of range. Left: A single source, Right: An array with 8 sources with 10 m spacing.**

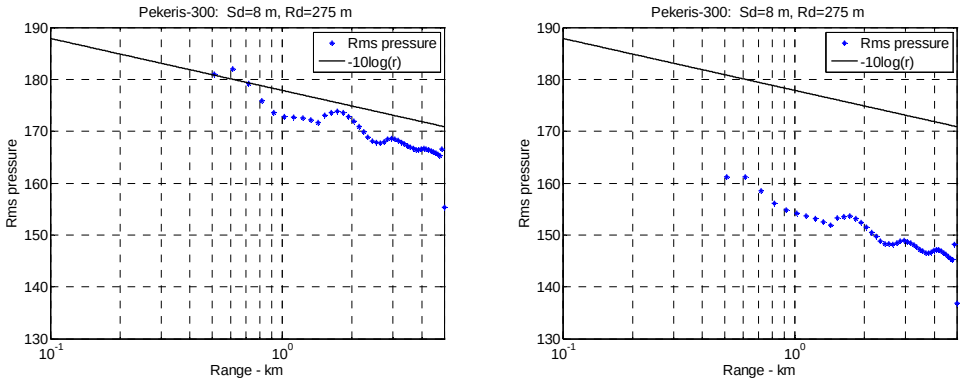

Figure 16 **Rms pressure as function of range. Left: A single source, Right: An array with 8 sources with 10 m spacing.**

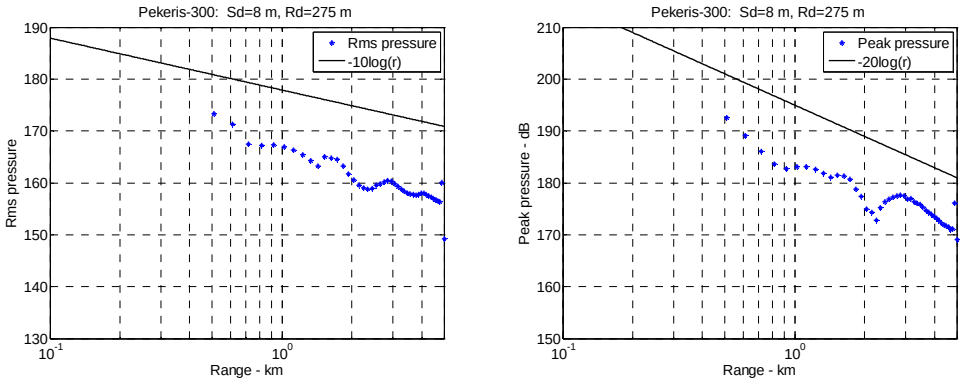

Figure 17 **Rms pressure and peak pressure as function of range for an array with 8 sources with 2.5 m spacing, receiver at 275 m depth 25 m above the bottom.**

4 Discussion and comments

The results show that the airgun signal propagating in a direction near vertical is essentially a single and sharp pulse since the pulses from all the individually sources add coherently in time. In all other directions the pulses from the individual sources are spread out in time. Consequently, the seismic signal transmitted to long distances starts with lower peak pressure than the vertically transmitted signal.

This model for directivity of air gun arrays is implemented in the PlaneRay code, but detailed in formation of the airgun arrays is needed for accurate evaluation of the effect of array directivity. The results and consequences are significant and important for the scaring effects on fish population caused by seismic noise.

Technology for a better society

www.sintef.no